Reversions mask the contribution of adaptive evolution in microbiomes

Paul A. Torrillo [1,2] and Tami D. Lieberman [1,2,3,4+]

[1] Institute for Medical Engineering and Sciences, Massachusetts Institute of Technology, Cambridge, MA 02139, USA
[2] Department of Civil and Environmental Engineering, Massachusetts Institute of Technology, Cambridge, MA 02139, USA
[3] Broad Institute of MIT and Harvard, Cambridge, MA 02139, USA
[4] Ragon Institute of MGH, MIT, and Harvard, Cambridge, MA 02139, USA

+ Please address correspondence to tami@mit.edu

Abstract

When examining bacterial genomes for evidence of past selection, the results obtained depend heavily on the mutational distance between chosen genomes. Even within a bacterial species, genomes separated by larger mutational distances exhibit stronger evidence of purifying selection as assessed by d_N/d_S, the normalized ratio of nonsynonymous to synonymous mutations. Here, we show that the classical interpretation of this scale-dependence, weak purifying selection, leads to problematic mutation accumulation when applied to available gut microbiome data. We propose an alternative, adaptive reversion model with exactly opposite implications for dynamical intuition and applications of d_N/d_S. Reversions that occur and sweep within-host populations are nearly guaranteed in microbiomes due to large population sizes, short generation times, and variable environments. Using analytical and simulation approaches, we show that adaptive reversion can explain the d_N/d_S decay given only dozens of locally-fluctuating selective pressures, which is realistic in the context of *Bacteroides* genomes. The success of the adaptive reversion model argues for interpreting low values of d_N/d_S obtained from long-time scales with caution, as they may emerge even when adaptive sweeps are frequent. Our work thus inverts the interpretation of an old observation in bacterial evolution, illustrates the potential of mutational reversions to shape genomic landscapes over time, and highlights the importance of studying bacterial genomic evolution on short time scales.

Introduction

Understanding evolutionary pressures acting upon bacterial populations is crucial for predicting the emergence and future virulence of pathogens [1], modeling strategies to combat antimicrobial resistance [2], and designing genetically modified organisms [3]. Bacteria can adapt at rapid rates due to their short generation times and large population sizes. Indeed, the rapid evolutionary potential of the microbiome has been proposed to assist in dietary transitions of mammals [4]. However, the vast majority of possible mutations do not increase bacterial

fitness and instead result in a neutral or a deleterious effect [5] [6] [7] [8]. Metrics that estimate the directionality and intensity of past selection at genomic loci of interest have thus become critical tools in modern microbiology and biology more generally.

The normalized ratio of nonsynonymous (N) to synonymous (S) substitutions, known as d_N/d_S or the K_A/K_S ratio, is a widely used indicator of past selection [9] [10] [11]. Nonsynonymous substitutions change the encoded amino acid and thus are considered likely to impact a protein's function, while synonymous substitutions do not affect the encoded amino acid and are therefore considered effectively neutral, with limited exceptions [12]. To account for the fact that nonsynonymous mutations are more likely than synonymous mutations based on the genomic code (~3X on average [13]), the values 'd_N' and 'd_S' normalize mutation counts to available sites on the genome. The d_N/d_S ratio therefore summarizes past selection on a genetic sequence, which could be a whole genome, pathway, gene, functional domain, or nucleotide; notably values of d_N/d_S averaged genome-wide can obscure signatures of adaptive evolution on other portions of the genome [14] [15] [16]. A d_N/d_S ratio of greater than 1 indicates the dominance of past adaptive evolution (i.e. directional selection) while a ratio of less than 1 traditionally implies past selection against amino acid change (purifying selection).

Early sequencing work comparing bacterial genomes of the same species reported relatively low d_N/d_S values across the whole genome (<0.15) [7] [8]. These observations, obtained from comparing distant bacteria within each species, indicated a strong predominance of purifying selection. However, as it became economically feasible to sequence organisms separated by fewer mutations and therefore less evolutionary time, a contrasting pattern emerged in which high d_N/d_S values (~1) were found between closely related strains [17] [18]. Recent work in the human microbiome has confirmed such results, and furthered the contrast between timescales by finding values of d_N/d_S greater than 1 [19] [20] [21]. The time scale dependence of d_N/d_S has been mainly attributed to the ongoing action of purifying selection [10] [19], a model first proposed by Rocha et al. [22]. According to this model, weak purifying selection (or locally inactive purifying selection [14]) allows for an initially inflated d_N/d_S ratio, as deleterious mutations that will eventually be purged still remain in the population. As time progresses and purifying selection continuously operates, the d_N/d_S ratio decreases [14] [19] [22]. However, multiple studies have observed genome-wide values of d_N/d_S above 1 in these same microbial systems, with values substantially above 1 in key genes, which are simply unaccounted for in the purifying model [19] [20] [23] [24] [25].

Here, we demonstrate fundamental flaws in the purifying selection model in the context of the large within-person population sizes typical to the human microbiome and many bacterial infections ($>10^{12}$ bacteria / person). We use analytical, simulation-based, and genomic approaches to support a contrasting model for the timescale dependence of d_N/d_S, in which adaptive evolution predominates but is not apparent on long time scales due to adaptive reversion. The comparative success of the reversion model suggests that study of closely related bacteria is needed to fully understand evolutionary dynamics.

Results

A model of purifying selection that fits the data reveals unrealistic parameters

Explaining the timescale dependence of d_N/d_S through an exclusively purifying selection model poses several challenges. Firstly, fitting observed data with purifying selection requires a preponderance of mutations with extraordinarily small effects on fitness (selective coefficients, s), which are challenging to eliminate effectively [26]. Secondly, the occurrence of an adaptive event during the extensive time required to purge weakly deleterious mutations interrupts the purification of such mutations. Lastly, neutral bottlenecking processes, such as those observed during host-to-host transmission, exacerbate the accumulation of deleterious mutations. For most of this section, we will disregard these last two complications and focus on the problem of small s. To provide clarity, we first detail the classic purifying selection model.

Mutations can be divided into three classes, the first two of which accumulate at a constant rate per unit time: synonymous mutations (S), neutral nonsynonymous mutations (N_{neut}), and nonneutral, transient, nonsynonymous mutations ($N_{transient}$). We restate the timescale dependence of d_N/d_S as the observation that, in a population starting from a single WT cell, the average number of nonneutral nonsynonymous mutations per cell in the population ($\overline{N}_{transient}$) increases and then asymptotes. The exclusive purifying selection model [19] [22] can now be written as:

$$\frac{d_N}{d_S} = \frac{\overline{N}_{neut} + \overline{N}_{transient}}{3\overline{S}} \quad (1) \qquad \text{and} \qquad d\overline{N}_{transient} = U_N dt - s\overline{N}_{transient} dt \quad (2)$$

Here, U_N is the nonneutral mutation rate per core genome per generation, s is the selective disadvantage of a nonneutral nonsynonymous mutation (or the harmonic mean of such mutations, SI Text 1.1) and t is the number of generations. The 3 in the denominator of (1) accounts for the discrepancy in the number of potential nonsynonymous and synonymous sites [13]. We solve for $\overline{N}_{transient}$ by assuming $\overline{N}_{transient}(t = 0) = 0$ to obtain:

$$\overline{N}_{transient}(t) = \frac{U_N(1-e^{-st})}{s} \quad (3)$$

We further simplify and combine these equations to create an equation for d_N/d_S with only two parameters as previously done [19]. First, since d_N/d_S plateaus with time (Fig. 1a), we have $\lim_{t \to \infty} \frac{\overline{N}_{neut} + \overline{N}_{transient}}{3\overline{S}} = \frac{\overline{N}_{neut}}{3\overline{S}} = \alpha$. Conveniently, α represents both the asymptote of d_N/d_S and the proportion of nonsynonymous mutations that are neutral. This allows us to leave only s as the other free parameter, obtaining (SI Text 1.1):

$$\frac{d_N}{d_S} = \alpha + (1 - \alpha)\frac{1-e^{-st}}{st} \quad (4)$$

As sequence analysis is not privy to the actual number of generations, we approximate t assuming that synonymous mutations accumulate according to a molecular clock ($t = \frac{dS}{2(1/4)\mu}$) where μ is the mutation rate per generation per base pair, ¼ represents the proportion of random mutations that are synonymous [13], and 2 accounts for fact that divergence is a measure between a pair of genomes. As selection and mutation are both in units of per time, any change in μ results in a corresponding change in s. Both model fits and consequences are largely dependent on the ratio of these two variables (more on this below), and thus are not sensitive to choice of μ. We use a relatively high mutation rate of 10^{-9} per base pair per generation [27] [28] as lower would imply even weaker purifying selection.

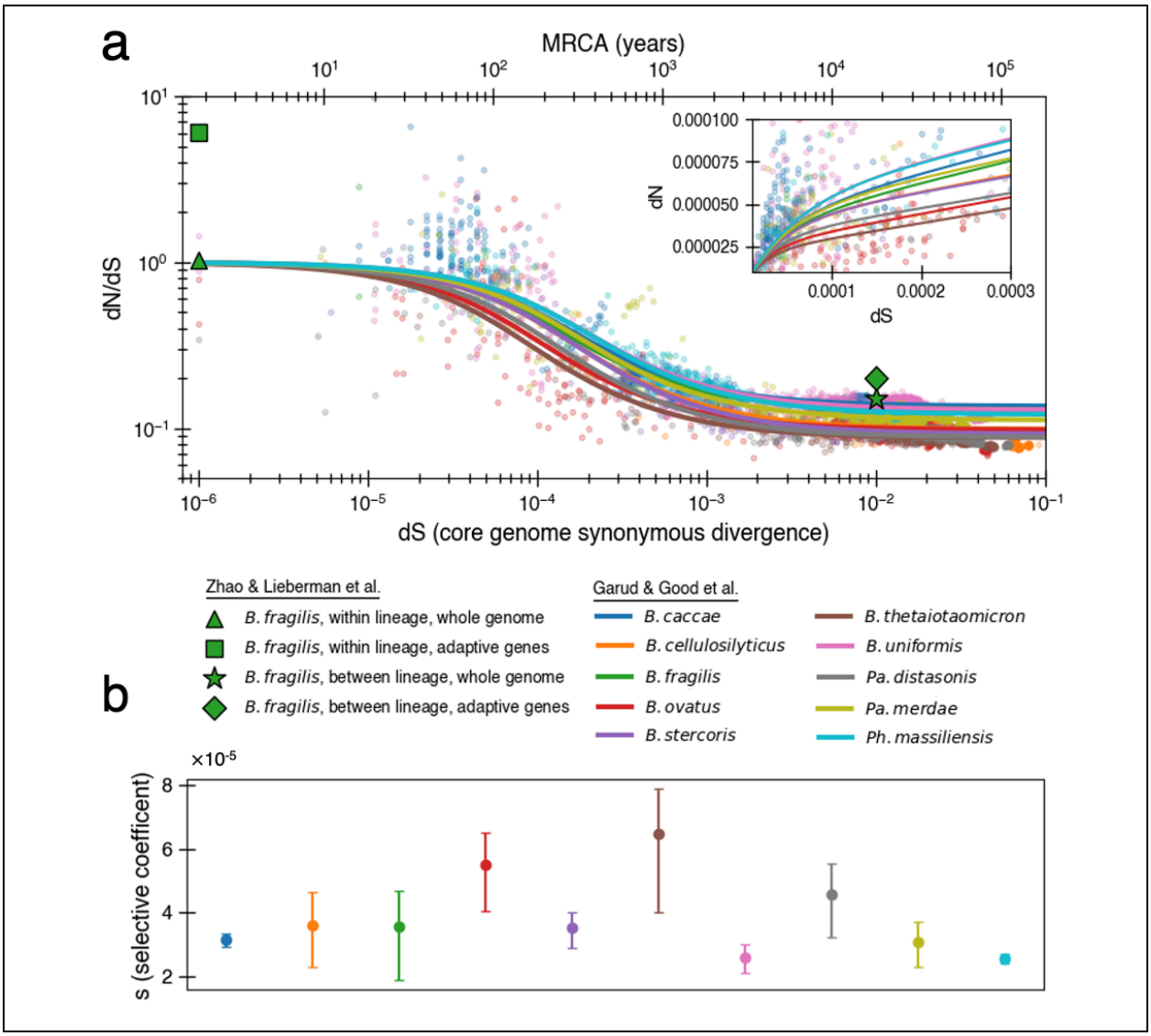

Figure 1: The previously proposed explanation for the time dependence of d_N/d_S is weak purifying selection. **(a)** Time-dependent signature of d_N/d_S as depicted by data points derived from the studies of Garud & Good et al. [19], and Zhao & Lieberman et al. [24]. Each dot represents a pairwise comparison between the consensus sequence from two gut microbiomes as computed by [19], using only the top ten species based on quality of data points (see Methods). Where the high initial value of d_N/d_S begins to become the low asymptotic value of d_N/d_S occurs at approximately $d_S = \frac{\mu_s}{s}$. Fit lines were derived from these points using equation (4) to depict the trend. The median R^2 is 0.81 (range 0.54-0.94). Corresponding data from [24] confirms these observed trends, demonstrating high levels of d_N/d_S at short time scales and low levels at longer time scales. Adaptive genes are from [24], and defined as those which have high d_N/d_S values in multiple lineages. *Insets:* d_N vs d_S on linear scale. Note that the data was fit to minimize variance in the logarithmic scale not the linear scale so the fit is not expected to be as good for the inset. See Fig. S1 for minimizing variance on a linear scale. See Fig. S2 for all species on separate panels. (**b**) Values of s from the output of 999 standard bootstrap iterations of curve fitting, conducted with replacement, demonstrate that only small values of the average selective coefficient can fit the data.

Fitting the data from Garud & Good et al [19], we infer median values of $\alpha \approx 0.10$ (0.09-0.14) and $s \approx 3.5 \times 10^{-5}$ (2.6×10^{-5}-6.5×10^{-5}) across all species (Methods, Fig. 1a). Aggregating all of the data at once results in a similar optimal fit of $\alpha \approx 0.11$ and $s \approx 2.8 \times 10^{-5}$. The similarity across the 10 species is perhaps not surprising, given that all are human gut residents of the order *Bacteroidales*; these values are also in line with values obtained previously from aggregating across all species [19]. These values indicate a model in which only ~10% of nonsynonymous mutations are neutral and the remaining ~90% are so weakly deleterious that they are beyond the limit of detection of any experimental method to date ($s \geqq 10^{-3}$) [29]. Higher values of s that better reflect experimental observations [30] [31] [32] result in poor fits to the data (Fig. S3). While the implied proportion of mutations that are deleterious may seem high, deep mutational scanning experiments have revealed that most amino-acid changing mutations in essential genes are deleterious enough to be measured in the lab [33] [34]; complex real-world environments are expected to constrain an even larger fraction of the genome.

In finite populations, the presence of so many weakly deleterious mutations becomes quickly problematic. When s is smaller than U_N, organisms without any deleterious mutations (or with the fewest number of deleterious mutations, the "least-loaded class" [26]) can be easily lost from a finite population before they outcompete less fit organisms and fitness decay begins to occur. The likelihood of loss depends on the population size and mutation-selection balance (U_N/s), a parameter which estimates the average number of deleterious mutations per cell relative to the least loaded-class. Given a core genome of $L = 1.5 \times 10^6$ bp that can acquire deleterious mutations, we then expect 0.001 new deleterious mutations per genome per generation ($U_N = \frac{3}{4}(1 - \alpha)L\mu$). Thus, the value of U_N/s for the above fits is ~29, indicating that most cells in the population contain dozens of deleterious mutations (SI Text 1.2). With this value of the mutation-selection balance parameter, the frequency of mutation-free organisms in a population is extremely small, even for a population which starts without any deleterious

mutations (< 10^{-12} after 100,000 generations). If the flexible genome also contains deleterious mutations, the least loaded class is pushed down even further. Simulations substantiate this prediction of mutation accumulation and decrease in frequency of the wild type (Fig. 2a, Methods).

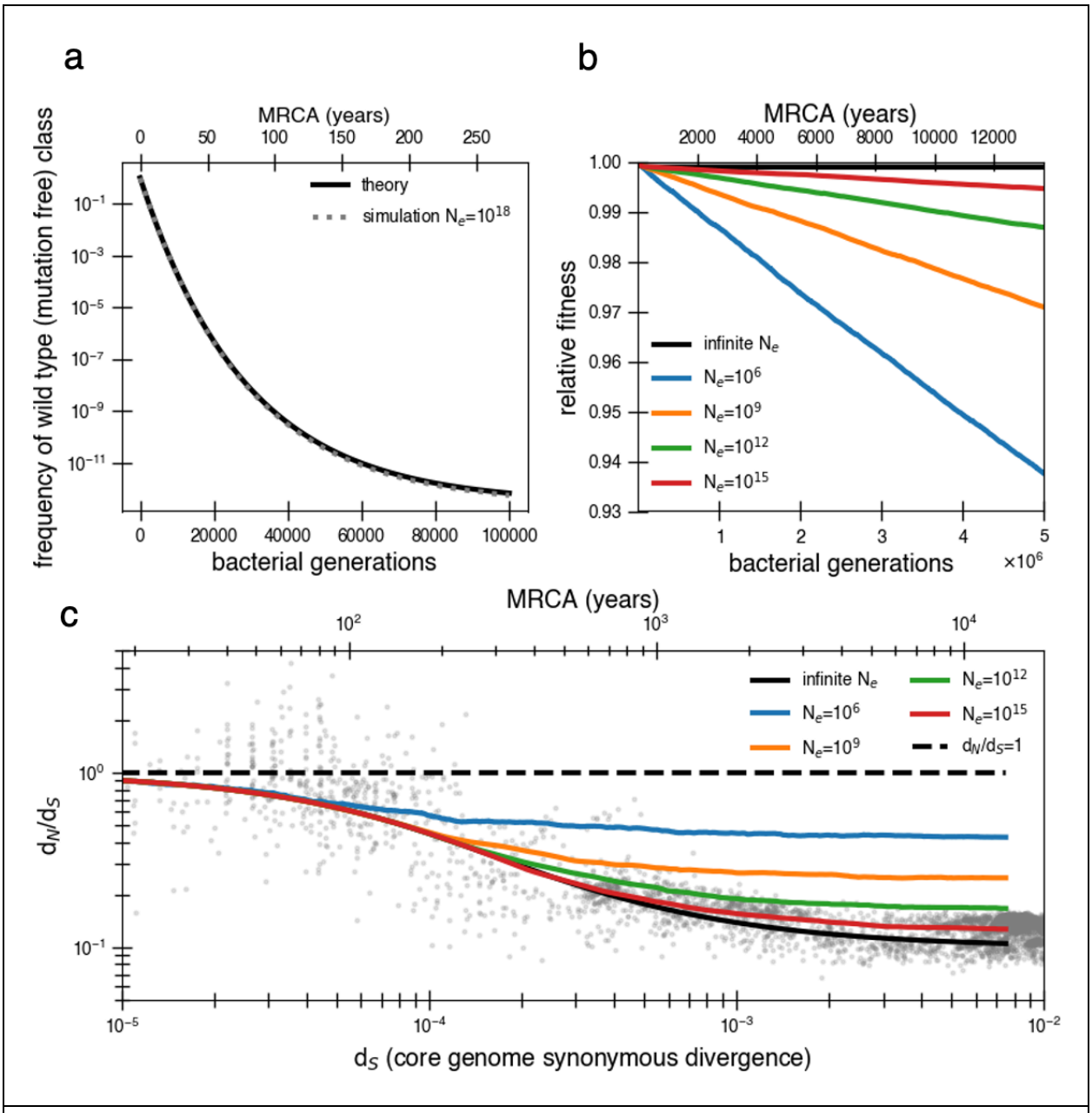

Figure 2: Models of extremely weak purifying selection that can fit the data suffer from mutation accumulation and fitness decay. (**a**) The temporal dynamics of the least-loaded class in a large population under the purifying selection model. The black line represents the predicted frequency of the wild-type (mutation-free) class over time. The simulation curve shows simulation results assuming constant purifying selection in an exceptionally large effective population size ($N_e=10^{18}$; see text for discussion of population size) under a slightly modified Wright-Fisher model (Methods). (**b**) As a consequence of the loss of the least-loaded class, fitness

declines in finite populations over time. Colored lines indicate simulations from various effective population sizes with mutations of constant selective effect. The deleterious mutation rate in the simulation is 1.01×10^{-3} per genome per generation. (**c**) Using the same simulations as in panel b, we see that realistic global effective population sizes fail to fit the d_N/d_S curve, with different asymptotes. The black line denotes the infinite population theoretical model, and the colored lines indicate increasing effective population sizes, which change the strength of genetic drift in the simulations. Larger values of s and models in which all mutations are deleterious cannot fit the data. (Fig. S4-S5). Generations are assumed to occur once every day.

The time until the least-loaded class is completely lost from the population depends on the strength of genetic drift. The strength of genetic drift is inversely proportional to population size in well-mixed populations [35], and in less well-mixed or otherwise non-ideal populations, is inversely proportional to a smaller parameter, the effective population size, N_e. N_e is often estimated by assessing polymorphisms in a population [35], but is hard to estimate from data following a recent bottleneck. Because each individual's gut microbiome is thought to be well mixed (census size = 10^{13}) [36], it has been recently argued that $N_e \approx 10^{11}$ reflects drift processes for dominant gut species [37] [38]. On the other hand, lower values of $N_e \approx 10^9$ or less have been estimated for global populations of bacteria [39] because of the slow rates of bacterial transmission across people. While this decrease in N_e when increasing scales may seem paradoxical, we note this use of N_e only reflects the magnitude of the force of drift; for other calculations in non-ideal populations, census population size or other parameters should be used.

Without extremely large values of N_e, the least-loaded class will be lost recurrently, rapidly lowering the fitness of the population (i.e. Muller's ratchet [26]). Assuming s is small and thus approximately additive, this recurrent process of fitness decay occurs roughly when the following inequality is satisfied (SI text 1.2) [40]:

$$2sN_e e^{-\frac{U_N}{s}} << 1 \quad (5)$$

Given $U_N/s = 29$ as derived above, $N_e > 10^{15}$ is required to avoid continual deleterious mutation accumulation and fitness decline (Fig. 2b). Thus, the purifying model requires levels of drift unrealistic at the within-person or across-globe scales. Simulations confirm that deleterious mutations accumulate and compromise the ability of the purifying model to explain empirical d_N/d_S decay in reasonably finite populations (Fig. 2c). Moreover, continuous accumulation of mutations in such populations decreases fitness so much that the average genome contains a sizable fraction (~10%) of deleterious alleles after 1 million years (Fig. 2c), assuming $N_e = 10^9$ and one generation a day [41]. Even if this decreased fitness was biologically maintainable, the accumulation of so many deleterious mutations would lead to many potential adaptive back mutations, complicating the efficiency of purifying selection. Consequently, this value of U_N/s is simply incompatible with a model where a vast majority of alleles are already optimal.

Lastly, the intolerance of the purifying model to adaptation and transmission is particularly problematic. Within-host adaptive sweeps have been observed in *Bacteroides fragilis* [24] and other *Bacteroides* [19]. Such adaptation interferes with inefficient purifying selection; deleterious mutations are likely to hitchhike [42] to fixation on the genomic background of

adaptive mutations. Any given weakly deleterious mutation with $s = 3.5 \times 10^{-5}$ cannot be purged from a within-host population on the timescale of human lifetime (assuming ~1 generation per day), and thus if any adaptive sweep occurred within that host, it would either hitchhike to fixation or be completely removed from the population. Similarly, deleterious mutations can also hitchhike to fixation during neutral transmission bottlenecks, thereby raising the average number of deleterious mutations per cell in the population, furthering mutation accumulation, and hampering the efficiency of purifying selection. Simulations confirm that even infrequent adaptive sweeps and bottlenecks have tangible impacts on d_N/d_S, including raising the asymptote (Fig. S6).

Neither recombination nor transmission can rescue the purifying model

Homologous recombination, which occurs at detectable rates within human gut microbiomes and within the *Bacteroidales* [43], cannot rescue a population from Muller's ratchet when such weakly deleterious mutations are so frequent. If we assume a generously high rate of recombination, such that a mutated nucleotide is 500 times more likely to be reverted via recombination than mutation (*r/m*=500) [44] [43] and brings along synonymous mutations during this recombination process, the decay of d_N/d_S still cannot be recreated in a population of size 10^9 and fitness will still decay (Fig. S7). The inability of recombination to suppress mutation accumulation in this regime arises because the selective advantages themselves are still too small to sweep faster than the rate at which mutations accumulate. While recombination does allow d_N/d_S to eventually decay, the rate of decay is much slower than observed, resulting in a poor fit to the data (Fig. S7). While higher values of N_e or a higher recombination rate could theoretically approximate the absence of linkage and escape of Muller's ratchet, we note that the maximum *r/m* across bacteria is estimated to be less than 50 [44] and our simulations are therefore conservative.

An alternative model, in which selective coefficients vary over time and purifying selection acts only during transmission (e.g. nonsynonymous mutations are neutral or adaptive in the host in which they arise [1] [14]) cannot prevent mutation accumulation without unrealistic assumptions. This selection-at-transmission model would still require ~29 nonneutral mutations in the average adult's population, which implies a very low frequency of the least-loaded class. Assuming each host's population gets replaced once every 10,000 bacterial generations (~26 years), such a model would require the least-loaded class to be 6,000X more likely to colonize them than the average genotype in the population ($(1 + 10,000s)^{29}$). The presence of rare cells with strong selective advantages would suggest super-spreading across human microbiomes, which has yet to be reported in the human microbiome [45]. More importantly, Muller's ratchet would still click because of the low frequency of this least-loaded class.

Adaptive reversions can explain the decay of d_N/d_S

If purifying selection can't explain the decay in neutral mutations, what can? One particularly attractive process which removes nonsynonymous mutations over time is strong

adaptive mutation and subsequent strong adaptive reversion of the same exact nucleotide when conditions change. Such reversions are likely to sweep in large populations when mutations are adaptive locally but deleterious in other environments [46]. In the gut microbiome, these alternative environments could represent different hosts (Fig. 3a) or environmental changes within a single host (e.g. diet, medication, other microbes). As an illustrative example, the presence of a bacteriophage in one gut microbiome might select for a loss-of-function mutation (premature stop codon or otherwise) in a phage receptor, driving this mutation to fixation in its host, but reverting to the wild-type receptor when transmitted to a phage-free host. Reversions are most likely when compensatory mutations which counteract a mutation's deleterious effects are either scarce or not as beneficial as direct reversion [47] (i.e. provided a premature stop codon); we discuss models that include compensatory mutations later in this section.

Adaptive nonsense mutations have been observed to emerge frequently within individual people in both pathogens [1] [20] [48] [49] and commensals [24] [50]. Identifying reversions *in vivo* requires both high temporal resolution and deep surveillance such that the probability of persistence of ancestral genotype is removed [51]; despite this difficulty reversions of stop codons have been observed in mouse models [52] and during an outbreak of a pathogen infecting the lungs of people with cystic fibrosis [53]. While direct reversion has not yet been observed in gut microbiomes, premature stop codons are frequently observed. Among the 325 observed nonsynonymous *de novo* mutations in a study of within-host *B. fragilis* adaptation [24], 28 were premature stop codons. This frequency is significantly higher than expected by chance ($p=0.015$; Methods). Moreover, 4 of the 44 mutations in 16 genes shown to be under adaptive evolution on this short time scale were stop codons. These same 16 genes show a signature of purifying selection on long time scales (Fig. 1a).

Traditionally, mutational reversions of stop codons and other mutations have been considered exceedingly unlikely and have been ignored in population genetics [54], with a few exceptions [55]. However, for a bacterial population within a human gut microbiome, the likelihood of a mutational reversion is actually quite high. A single species within the gut microbiome can have a census population size of 10^{13}, with generation rates ranging from 1-10 per day [36] [41]. Taking a conservative estimate of 1 generation per day and a within-person N_e of 10^{10} (e.g. bacteria at the end of the colon may not contribute much to the next generation [38]) reversions become highly probable (Fig. 3b; SI Text 2). Given a mutation rate of 10^{-9} per site per generation, we anticipate 10 mutants at any given site each generation. In the large population sizes relevant for the gut microbiome, a beneficial mutation will then take substantially longer to sweep the population than occur, with values of $s_{ben} > 1\%$ generally sweeping within 10 years (Fig. 3b). Consequently, if selection strongly benefits a reverting mutation, a genotype with a beneficial mutation is essentially guaranteed to emerge within days to weeks and replace its ancestors within the host within months to years.

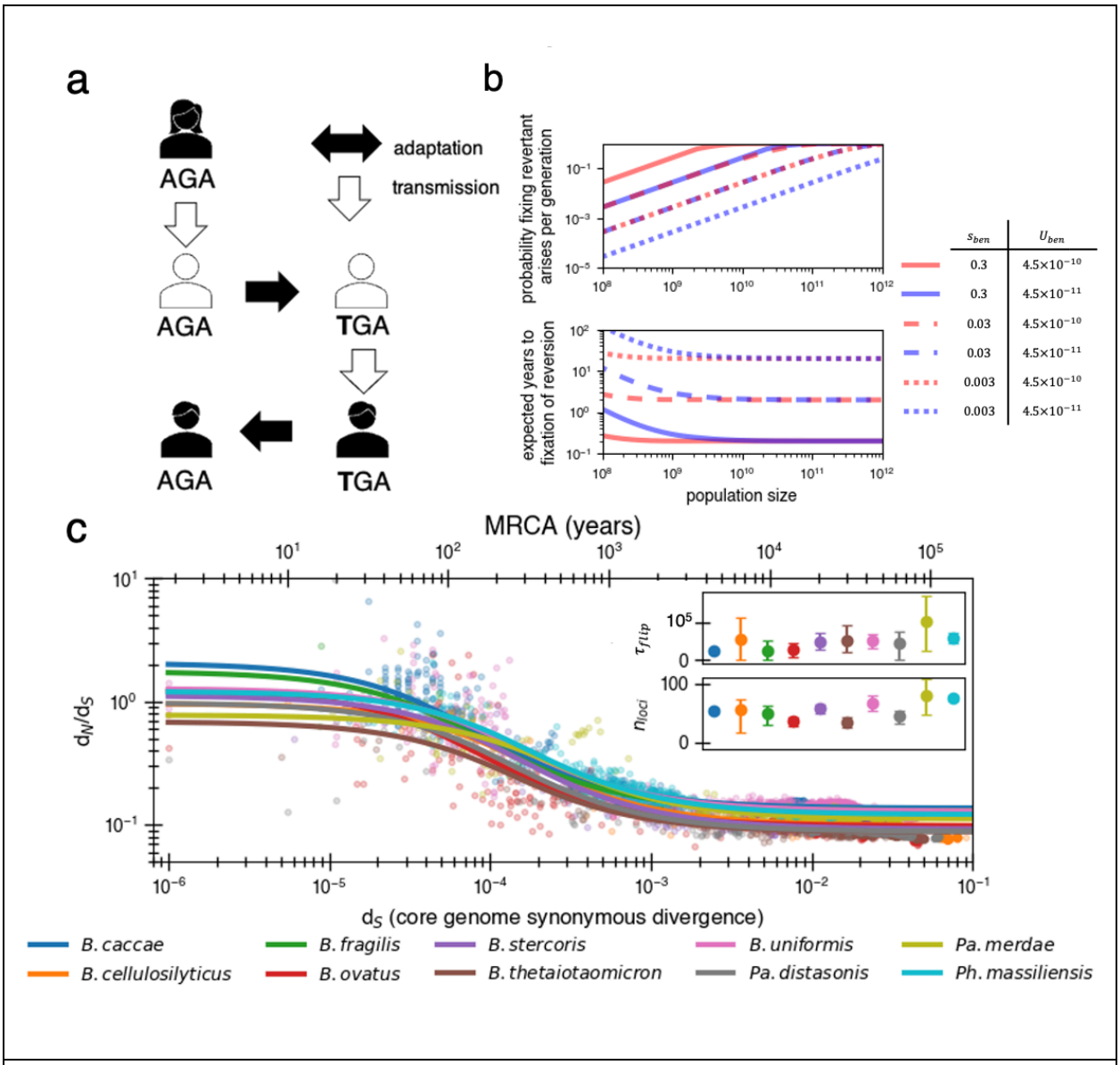

Figure 3: Locally adaptive mutations and subsequent reversions can explain the decay of nonsynonymous mutations. (**a**) Cartoon schematic depicting a potential reversion event within a single transmitted lineage of bacteria. The color of each individual indicates a different local adaptive pressure. Closed arrows represent mutation while open arrows indicate transmission. (**b**) Reversions become increasingly likely at larger population sizes, and nearly guaranteed to occur and fix within 1-10 years when strongly beneficial in gut microbiomes. Probability of revertant arising and fixing (top panel) is calculated as $1 - (1 - 2s_{ben}U_{rev})^{N_e}$ and expected time to fixation of reversion (bottom panel) is calculated as $\frac{1}{2N_e s_{ben} U_{rev}} + \frac{ln(N_e)}{s_{ben}}$ ($U_{rev} = 4.5 \times 10^{-10}$ per generation). Generation times are assumed to be 1 day. Note that mutation rate does not affect time to fixation much when N_e is large. Here we assume no clonal interference or bottlenecks, though simulations do take these processes into account. See SI Text 2.2 for derivation. Each line type displays a different selective advantage coefficient. (**c**) The adaptive reversion model can fit the data. Each colored line shows the fit for a different species. The median $R^2 = 0.82$ (range 0.54-0.94). Fit minimizes logarithmic variance. See Fig. S8 for alternative

fitting linear variance. See Fig. S9 for species individually. *Insets:* Fit parameters for τ_{flip}, the average number of generations for *a given* environmental pressure to switch directions and n_{loci}, the average number of sites under different fluctuating environmental pressures. The scale of the y axis is linear. Confidence intervals are from 999 bootstrapped resamples.

Given its plausibility, we now consider if the reversion model can explain observed decay of d_N/d_S. The dynamics of the reversion model can be given by:

$$\frac{d\overline{N}_{transient}}{dt} = \frac{1}{\tau_{flip}}(n_{loci} - \overline{N}_{transient}) - \frac{1}{\tau_{flip}}\overline{N}_{transient} \quad (6)$$

With the corresponding solution for $\overline{N}_{transient}$ being (SI Text 3.1):

$$\overline{N}_{transient}(t) = \frac{n_{loci}}{2}(1 - e^{-\frac{2t}{\tau_{flip}}}) \quad (7)$$

Here, n_{loci} denotes the number of loci which experience distinct sources of fluctuating selection. The parameter τ_{flip} represents the average number of generations required for the sign of selection at a chosen locus to flip, and determines the key point in the d_N/d_S decay curve where $\overline{N}_{transient}(t)$ begins to drop. We note that a locus here could be a nucleotide, gene, or gene set -- any contiguous or non-contiguous stretch of DNA in which two knockout-mutations would be just as beneficial or harmful as one mutation. We again use α to represent the proportion of non-synonymous mutations that are neutral. Using equation (7), we obtain a formula for d_N/d_S that has only three free parameters when a single value for μ_S is chosen:

$$\frac{d_N}{d_S} = \alpha + \frac{n_{loci}}{6\mu_S t}(1 - e^{-\frac{2t}{\tau_{flip}}}) \quad (8)$$

When fitting the d_N/d_S curve, the values obtained are reasonable in the context of bacterial genomics, with median best fit values across species of τ_{flip} = 46,200 bacterial generations (Range: 24,900-105,000) and n_{loci} = 55 (Range: 34-80). Given daily bacterial generations, this value of τ_{flip} suggests the sign of selection on a given allele would flip approximately every 110 years. The average time for any pressure to flip would thus be approximately every two years, or less frequently if adaptive events occur in bursts (e.g. upon transmission to a new host). While 55 loci under distinct selective pressures may seem high, *Bacteroidetes* genomes are known to have dozens of invertible promoters (up to 47 in *Bacteroides fragilis* [56]). Invertible promoters are restricted out of the genome and re-ligated in the opposite direction to turn gene expression on or

off. The number of invertible promoters in a given genome approximates a lower bound on the number of fluctuating selective pressures that these genomes frequently experience. Interestingly, adaptive loss-of-function mutations reported in *B. fragilis* affect the same genes regulated by invertible promoters [24]. The plausibility of these fit parameters lends support to a model in which d_N/d_S decays solely based on strong and recurrent local adaptations.

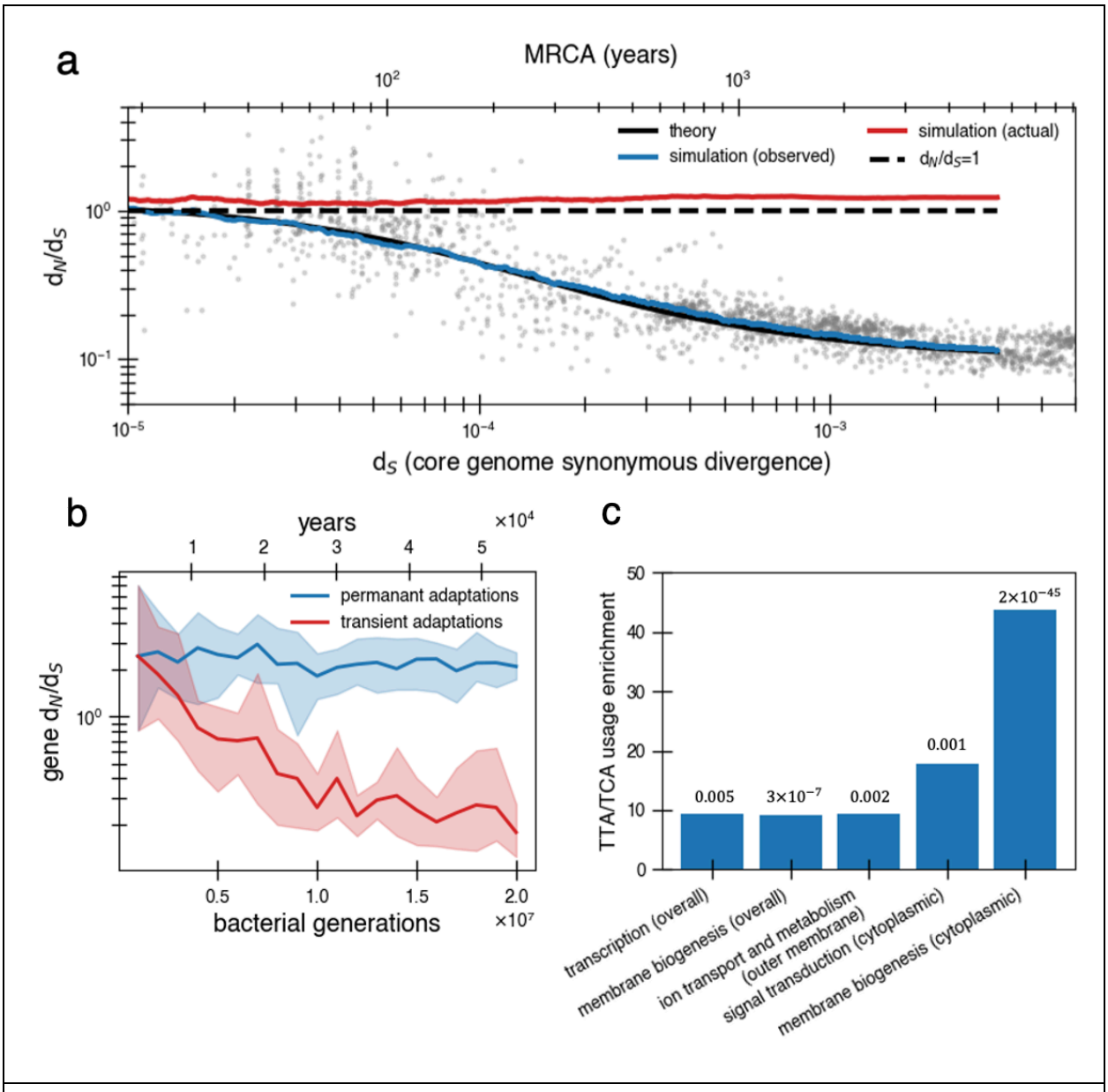

Figure 4: Under a model of reversion, the apparent d_N/d_S on long timescales underestimates the extent of adaptive evolution. (**a**) The reversion model successfully fits the data in simulations. We simulate a population of size 10^{10} that has a bottleneck to size 10 on average every 10,000 generations (~27 years or a human generation [57] given a bacterial generation a day), with one beneficial mutation ($s_{ben} = 0.03$) occurring on average every 840 generations independently of bottlenecks (see Fig. S10 for alternative where bottlenecks and selection are

correlated). Available beneficial mutations are either forward mutations (which can be acquired at a rate of 1.1×10^{-8} per available locus per generation) or reversions (which can be acquired at a rate of 4.5×10^{-10} per available locus per generation) or, the balance of which depends on the history of mutations taken by the tracked genome (i.e. more past forward mutations implies more potential future reversions). Based on the best fit to the data we use $n_{loci} = 55$. Deleterious mutations occur at a rate of 1.01×10^{-3} mutations per genome and have $s = 0.003$ and can themselves be reverted. More details on the simulation can be found in Methods. Each curve represents the average of 10 runs; the blue line shows the observed pairwise d_N/d_S while the red line includes adaptive mutations and reversions. The theory line is the result of equation (8). Observable d_N/d_S decays because of reversion, while the actual d_N/d_S of mutations that occurred is above one when taking into account both forward and reverse mutations. (**b**) PAML [58] cannot detect true d_N/d_S in a given gene in the presence of adaptive reversions. Both lines are d_N/d_S as calculated by PAML on a simulated gene phylogeny. In the permanent adaptations simulation (blue), adaptive mutations are acquired simply and permanently. In the transient adaptations simulation (red), only more recent mutations will be visible while older mutations are obscured (Methods). Line is the average of ten simulated phylogenies and shaded regions show the range. (**c**) Categories of genes in the *Bacteroides fragilis* genome (NCTC_9343) enriched for stop-codon adjacent codons (TTA and TCA) relative to the expectation from the rest of the genome (Methods). The use of these codons suggests these sequences may have recently had premature stop codon mutations. P values are displayed above bars and were calculated using a one-proportion Z test with Bonferroni correction. See Methods, SI Table 1, and SI Table 2 for more details.

To ensure a reversion model is robust to finite populations, we performed simulations using fit parameters. These simulations capture the dynamics of a single population evolving as it transmits across a series of hosts through random bottlenecks (Fig. 4a; Methods); these simulations allow for clonal interference between adaptive mutations. We allow new pressures to arise independent of bottlenecks, as new selective forces (phage migration [59]; immune pressures [60]; dietary changes [61]) can emerge throughout the lifespan and independent of migration; forcing transmission and bottlenecks to coincide gives similar results (Fig. S8). As in the purifying selection simulations, the per-base pair mutation rate is 10^{-9} and 90% of nonsynonymous substitutions are deleterious, but this time they have a larger s of 0.003 [32] and are thus purged more quickly from the population. Notably, while some of these deleterious mutations hitchhike to fixation during bottlenecks and adaptive sweeps, fitness does not decay because these mutations are subsequently reverted with adaptive sweeps (Fig. S12). If deleterious mutations had a significantly smaller s, they would be unable to be reverted due to the long time needed to reach fixation, even if bottlenecks and adaptive events are less frequent (Fig. S7).

We note that other complex models that include reversion and other processes are also possible. For example, a model with a very large number of loci with selective tradeoffs, and pressures that act only transiently (non-fluctuating) could potentially fit the data. However, the agreement between n_{loci} and the number of invertible promoters, and the finding of parallel evolution in vivo, suggests the fluctuating selection model is more realistic than a very many sites model.

So far, we have assumed that only exact reversions are selected upon when the sign of selection returns to its original state. However, the reversion model can also accommodate compensatory mutations which exclude any selective advantage for reversion; these compensatory mutations can also be subject to reversion themselves. We conceptualize this as a random walk, in which a locus at a non-ancestral state acquires a compensatory mutation with probability p or obtains a true reversion with probability $1 - p$ (SI Text 3.2). As long as $p \leq 0.5$, d_N/d_S will decay to the same asymptote despite adaptive dynamics occurring. While compensatory mutations shift the timing of d_N/d_S decay to the right, it can be shifted backwards by decreasing n_{loci} (Fig. S13a). The condition $p \leq 0.5$ is easily met when $s_{ben} = 0.03$, until excluding compensatory mutations are 10 times more likely than true reversion and provide 95% of the selective advantage of the true reversion (Fig. S13b). If selective pressures are stronger (as they might be in the presence of phage), true reversions will outcompete compensatory mutations even if the supply of compensatory mutations is greater or such mutations provide better relative compensation.

A critical consequence of the reversion model is that apparent and actual d_N/d_S values diverge quickly. Even when the true genome-wide d_N/d_S exceeds 1-- meaning that adaptive sweeps have been a dominant force in shaping genomes -- the observed value can be close to 0.1 on long timescales. This disparity complicates the interpretation of d_N/d_S, as it becomes challenging to determine whether a genome or gene lacks nonsynonymous mutations due to reversions or negative selection. We confirmed the inability to detect adaptive selection on a gene when reversion is rampant by simulating protein phylogenies; even the advanced software PAML (Phylogenetic Analysis by Maximum Likelihood) [58] significantly underestimates actual d_N/d_S (Fig. 4b; Methods). Without sufficient temporal sampling, no software can realistically estimate these hidden, adaptively driven nonsynonymous mutations.

Lastly, we sought to find evidence of past reversions of stop codons in certain genes by analyzing codon usage. Both leucine and serine have the property that they can be encoded by six codons, only one of which is highly stop codon adjacent (TTA for leucine and TCA for serine). Across the *B. fragilis* genome, these codons are depleted overall (13.48% usage rather than neutral expectation of 16.67%). However, specific COG categories are enriched in TTA and TCA codons relative to this baseline, including genes associated with transcription and cell envelope biogenesis (Fig. 4c, Methods, Table S1). Further, when functionally annotated genes are further categorized by cellular localization, more gene categories exhibit enrichment (Fig. 4c, Methods, Table S1), most notably genes involved in inorganic ion transport and metabolism which are localized to the outer membrane. Genes implicated in within-host *B. fragilis* adaptation [24] are also found disproportionately in this category of outer membrane transporters ($p=1.22 \times 10^{-4}$) Methods, Table S1). Both the cell envelope and membrane-bound transporters are known to mediate interactions with the immune system and phage [62] [63], and are therefore expected to experience fluctuating selective pressures. The enrichment of stop-codon adjacent codons in pathways associated with environment-dependent costs further supports a model in which adaptive mutational reversions are frequent.

Discussion

In this study, we present a new interpretation of the time-dependent changes in d_N/d_S for bacterial populations. We show that the traditional weak purifying selection model struggles to replicate theoretical results in realistic population sizes, and propose an alternative model with exactly opposite implications that is supported by analytical, simulation, and genomic results. Together, these results challenge the conventional view that high d_N/d_S values on short timescales are an artifact and should not be trusted. Instead, the success of the reversion model suggests that adaptive dynamics are underestimated on long time scales because of saturation of d_N.

It is perhaps not surprising that reversions have been relatively overlooked in previous literature. First, most population genetics theory focuses on eukaryotic organisms with smaller population sizes and longer generation times, for which reversion is less likely. The low likelihood of reversion in these populations has inspired the use of the convenient infinite-site model [54], which assumes that reversions never occur and simplifies derivations. While smaller values of N_e can be appropriate for modeling global bacterial dynamics-- because bottlenecks and geography limit how many organisms effectively compete--they are inappropriate for within-gut populations, which are less structured. While gut microbiomes do have spatial structure that reduces competition, theoretical work modeling this biogeography suggests that the census and active population sizes differ only ~10-fold [37] [38]. This brings the within-gut microbiome N_e to substantially larger than the per-nucleotide mutation rate, invalidating the infinite sites model. Secondly, while bacterial geneticists have long observed adaptive loss-of-function mutations, two common misinterpretations of population genetic parameters can underestimate the probability of reversion: molecular clock rates (μ), which are generally low, can easily be confused with the supply of potential mutations (μN_e) [64]; and classical approaches that assess N_e from genetic diversity vastly underestimate the currently active population size, particularly if a bottleneck recently occurred (e.g. during transmission). Lastly, simulating large populations, even when appropriate, is computationally difficult. As a consequence, population genetics simulations, including those of bacteria, have used relatively small population sizes ($\leq 10^6$ organisms). We overcome computational limitations by tracking genetic classes rather than individual genotypes (Methods). While our approach does not allow explicit comparison between individuals within a population, we believe this framework represents a powerful method to simulate large population sizes when applicable.

Whether or not a reversion model can be applied beyond host-associated microbial populations remains to be explored. We only analyze microbiome data here, but we anticipate that analyses of highly-curated d_N/d_S decay curves from microbial pathogens could yield similarly plausible parameter fits for the reversion model given past observations of d_N/d_S decay [22]. When effective population sizes are smaller than 10^9 reversions are relatively unlikely. For example, while adaptive reversions can sweep individual gut microbiomes, we do not propose that reversions sweep the global bacterial population. Regardless, theoretical work on animal populations has shown that adaptive reversions are possible after local population bottlenecks [55]. Similarly, environmental variations that change more rapidly than the timescale required for

a local selective sweep (e.g. those imposed by daily dietary changes in the gut; or imposed by light-dark cycles in the environment) would be less likely to drive fixation and subsequent reversion than the less rapid changes considered here (e.g. phage migration) [65]. On the other hand, adaptive reversions may be particularly relevant for viral populations, which are known to undergo within-host adaptation, have very large population sizes, and experience frequent bottlenecks [66]. In fact, reversions have commonly been observed in certain regions of the HIV genome, and have been postulated to diminish measured substitution rates in those regions [67].

Despite the success of a model of reversion alone in explaining d_N/d_S decay, it remains possible that other forces could additionally contribute. While we have shown that purifying selection alone, either continuously or during transmission, cannot explain d_N/d_S decay alone, it is possible that some degree of purifying selection could act alongside a reversion model. Similarly, directional selection could be incorporated into the reversion model by adjusting the parameter α. While the true contribution of adaptive evolution to α is likely non-zero, it is difficult to fit with available data and it is therefore left for future work.

While we have shown that recombination is unlikely to rescue the purifying selection model, we note that recombination with ancestral genotypes could drive adaptive reversions. Microbial geneticists have frequently observed that recombined regions exhibit lower d_N/d_S values compared to non-recombined regions [68], a signature consistent with having already experienced reversion or purifying selection. Recombination could potentially revert multiple mutations at specific loci simultaneously, which might be particularly beneficial in the presence of genomic epistasis. Thus despite the success of the mutation-driven model, it is likely that recombination plays some role in the decay of d_N/d_S.

While more direct observation of adaptive reversions is currently lacking, we propose that this paucity is simply an artifact of lacking samples along a line of descent with sufficient genomic resolution. Despite this challenge in observation, a recent study tracking *de novo* mutations between mothers and infants revealed several cases of apparent reversion, with elevated values of d_N/d_S above 1, though not significantly so [69]. Moreover, many short-term studies in the gut microbiome and beyond have revealed strong evidence of within-person adaptation, including parallel evolution [20] [23] [24] [70] and loss-of-function changes like premature stop codons [48] -- with low long-term d_N/d_S values in these same short-term genes [71]. We note that adaptation and reversion does not result in parallel evolution in the genomic record if various initial mutations result in the same phenotype (i.e. loss of function mutations); however, it would result in changes in codon-usage bias we have shown (Fig. 4c).

The shortcomings of the purifying model and success of the reversion model under realistic assumptions highlight the importance of studying evolution in real time for understanding evolutionary dynamics. In addition, our results highlight the importance of simulating large population sizes for explaining observations in bacterial population genomics, spotlight the potential for strong adaptation in bacterial populations, and underscore the need for continued development of population genetics theory for microbial populations.

References

[1] M. J. Culyba and D. Van Tyne, “Bacterial evolution during human infection: Adapt and live or adapt and die,” *PLoS Pathog.*, vol. 17, no. 9, p. e1009872, Sep. 2021.

[2] J. Davies and D. Davies, “Origins and evolution of antibiotic resistance,” *Microbiol. Mol. Biol. Rev.*, vol. 74, no. 3, pp. 417–433, Sep. 2010.

[3] S. D. Castle, C. S. Grierson, and T. E. Gorochowski, “Towards an engineering theory of evolution,” *Nat. Commun.*, vol. 12, no. 1, p. 3326, Jun. 2021.

[4] O. Kolodny and H. Schulenburg, “Microbiome-mediated plasticity directs host evolution along several distinct time scales,” *Philos. Trans. R. Soc. Lond. B Biol. Sci.*, vol. 375, no. 1808, p. 20190589, Sep. 2020.

[5] M. Kimura, “Preponderance of synonymous changes as evidence for the neutral theory of molecular evolution,” *Nature*, vol. 267, no. 5608, pp. 275–276, May 1977.

[6] E. K. Davies, A. D. Peters, and P. D. Keightley, “High frequency of cryptic deleterious mutations in Caenorhabditis elegans,” *Science*, vol. 285, no. 5434, pp. 1748–1751, Sep. 1999.

[7] K. A. Jolley *et al.*, “Carried meningococci in the Czech Republic: a diverse recombining population,” *J. Clin. Microbiol.*, vol. 38, no. 12, pp. 4492–4498, Dec. 2000.

[8] K. E. Dingle *et al.*, “Multilocus sequence typing system for Campylobacter jejuni,” *J. Clin. Microbiol.*, vol. 39, no. 1, pp. 14–23, Jan. 2001.

[9] T. H. Jukes, C. R. Cantor, and Others, “Evolution of protein molecules,” *Mammalian protein metabolism*, vol. 3, no. 24, pp. 21–132, 1969.

[10] S. Kryazhimskiy and J. B. Plotkin, “The population genetics of dN/dS,” *PLoS Genet.*, vol. 4, no. 12, p. e1000304, Dec. 2008.

[11] M. F. Barber and N. C. Elde, “Escape from bacterial iron piracy through rapid evolution of transferrin,” *Science*, vol. 346, no. 6215, pp. 1362–1366, Dec. 2014.

[12] K. Nowick, M. B. Walter Costa, C. Höner Zu Siederdissen, and P. F. Stadler, “Selection Pressures on RNA Sequences and Structures,” *Evolutionary bioinformatics online*, vol. 15. p. 1176934319871919, Aug. 29, 2019.

[13] Z. Yang and R. Nielsen, “Estimating synonymous and nonsynonymous substitution rates under realistic evolutionary models,” *Mol. Biol. Evol.*, vol. 17, no. 1, pp. 32–43, Jan. 2000.

[14] S. L. Loo, A. Ong, W. Kyaw, L. M. Thibaut, R. Lan, and M. M. Tanaka, “Nonsynonymous Polymorphism Counts in Bacterial Genomes: a Comparative Examination,” *Appl. Environ. Microbiol.*, vol. 87, no. 1, Dec. 2020, doi: 10.1128/AEM.02002-20.

[15] S. Y. W. Ho, M. J. Phillips, A. Cooper, and A. J. Drummond, “Time dependency of molecular rate estimates and systematic overestimation of recent divergence times,” *Mol. Biol. Evol.*, vol. 22, no. 7, pp. 1561–1568, Jul. 2005.

[16] G. I. Peterson and J. Masel, “Quantitative prediction of molecular clock and ka/ks at short timescales,” *Mol. Biol. Evol.*, vol. 26, no. 11, pp. 2595–2603, Nov. 2009.

[17] E. J. Feil *et al.*, “How clonal is Staphylococcus aureus?,” *J. Bacteriol.*, vol. 185, no. 11, pp. 3307–3316, Jun. 2003.

[18] L. Baker, T. Brown, M. C. Maiden, and F. Drobniewski, “Silent nucleotide polymorphisms and a phylogeny for Mycobacterium tuberculosis,” *Emerg. Infect. Dis.*, vol. 10, no. 9, pp. 1568–1577, Sep. 2004.

[19] N. R. Garud, B. H. Good, O. Hallatschek, and K. S. Pollard, “Evolutionary dynamics of bacteria in the gut microbiome within and across hosts,” *PLoS Biol.*, vol. 17, no. 1, p.

e3000102, Jan. 2019.
[20] T. D. Lieberman *et al.*, “Parallel bacterial evolution within multiple patients identifies candidate pathogenicity genes,” *Nat. Genet.*, vol. 43, no. 12, pp. 1275–1280, Nov. 2011.
[21] W. R. Shoemaker, D. Chen, and N. R. Garud, “Comparative Population Genetics in the Human Gut Microbiome,” *Genome Biol. Evol.*, vol. 14, no. 1, Jan. 2022, doi: 10.1093/gbe/evab116.
[22] E. P. C. Rocha *et al.*, “Comparisons of dN/dS are time dependent for closely related bacterial genomes,” *J. Theor. Biol.*, vol. 239, no. 2, pp. 226–235, Mar. 2006.
[23] R. L. Marvig, L. M. Sommer, S. Molin, and H. K. Johansen, “Convergent evolution and adaptation of Pseudomonas aeruginosa within patients with cystic fibrosis,” *Nat. Genet.*, vol. 47, no. 1, pp. 57–64, Jan. 2015.
[24] S. Zhao *et al.*, “Adaptive Evolution within Gut Microbiomes of Healthy People,” *Cell Host Microbe*, vol. 25, no. 5, pp. 656–667.e8, May 2019.
[25] S. Zhao, C. L. Dai, E. D. Evans, Z. Lu, and E. J. Alm, “Tracking strains predicts personal microbiomes and reveals recent adaptive evolution,” *bioRxiv*, p. 2020.09.14.296970, Sep. 15, 2020. doi: 10.1101/2020.09.14.296970.
[26] J. Haigh, “The accumulation of deleterious genes in a population--Muller’s Ratchet,” *Theor. Popul. Biol.*, vol. 14, no. 2, pp. 251–267, Oct. 1978.
[27] J. W. Drake, “A constant rate of spontaneous mutation in DNA-based microbes,” *Proc. Natl. Acad. Sci. U. S. A.*, vol. 88, no. 16, pp. 7160–7164, Aug. 1991.
[28] J. E. Barrick and R. E. Lenski, “Genome dynamics during experimental evolution,” *Nat. Rev. Genet.*, vol. 14, no. 12, pp. 827–839, Dec. 2013.
[29] R. Gallet, T. F. Cooper, S. F. Elena, and T. Lenormand, “Measuring selection coefficients below 10(-3): method, questions, and prospects,” *Genetics*, vol. 190, no. 1, pp. 175–186, Jan. 2012.
[30] T. T. Kibota and M. Lynch, “Estimate of the genomic mutation rate deleterious to overall fitness in E. coli,” *Nature*, vol. 381, no. 6584, pp. 694–696, Jun. 1996.
[31] S. Trindade, L. Perfeito, and I. Gordo, “Rate and effects of spontaneous mutations that affect fitness in mutator Escherichia coli,” *Philos. Trans. R. Soc. Lond. B Biol. Sci.*, vol. 365, no. 1544, pp. 1177–1186, Apr. 2010.
[32] L. Robert, J. Ollion, J. Robert, X. Song, I. Matic, and M. Elez, “Mutation dynamics and fitness effects followed in single cells,” *Science*, vol. 359, no. 6381, pp. 1283–1286, Mar. 2018.
[33] E. D. Kelsic, H. Chung, N. Cohen, J. Park, H. H. Wang, and R. Kishony, “RNA Structural Determinants of Optimal Codons Revealed by MAGE-Seq,” *Cell Syst*, vol. 3, no. 6, pp. 563–571.e6, Dec. 2016.
[34] L. Dewachter *et al.*, “Deep mutational scanning of essential bacterial proteins can guide antibiotic development,” *Nat. Commun.*, vol. 14, no. 1, p. 241, Jan. 2023.
[35] J. H. Gillespie, *Population Genetics: A Concise Guide*. JHU Press, 2004.
[36] R. Sender, S. Fuchs, and R. Milo, “Revised Estimates for the Number of Human and Bacteria Cells in the Body,” *PLoS Biol.*, vol. 14, no. 8, p. e1002533, Aug. 2016.
[37] O. M. Ghosh and B. H. Good, “Emergent evolutionary forces in spatial models of luminal growth and their application to the human gut microbiota,” *Proc. Natl. Acad. Sci. U. S. A.*, vol. 119, no. 28, p. e2114931119, Jul. 2022.
[38] D. Labavić, C. Loverdo, and A.-F. Bitbol, “Hydrodynamic flow and concentration gradients in the gut enhance neutral bacterial diversity,” *Proc. Natl. Acad. Sci. U. S. A.*, vol. 119, no.

1, Jan. 2022, doi: 10.1073/pnas.2108671119.
[39] L.-M. Bobay and H. Ochman, “Factors driving effective population size and pan-genome evolution in bacteria,” *BMC Evol. Biol.*, vol. 18, no. 1, p. 153, Oct. 2018.
[40] R. A. Neher and B. I. Shraiman, “Fluctuations of fitness distributions and the rate of Muller’s ratchet,” *Genetics*, vol. 191, no. 4, pp. 1283–1293, Aug. 2012.
[41] T. Korem *et al.*, “Growth dynamics of gut microbiota in health and disease inferred from single metagenomic samples,” *Science*, vol. 349, no. 6252, pp. 1101–1106, Sep. 2015.
[42] M. M. Desai, A. M. Walczak, and D. S. Fisher, “Genetic diversity and the structure of genealogies in rapidly adapting populations,” *Genetics*, vol. 193, no. 2, pp. 565–585, Feb. 2013.
[43] Z. Liu and B. H. Good, “Dynamics of bacterial recombination in the human gut microbiome,” *PLoS Biol.*, vol. 22, no. 2, p. e3002472, Feb. 2024.
[44] E. L. Torrance, C. Burton, A. Diop, and L.-M. Bobay, “Evolution of homologous recombination rates across bacteria,” *Proc. Natl. Acad. Sci. U. S. A.*, vol. 121, no. 18, p. e2316302121, Apr. 2024.
[45] J. J. Faith *et al.*, “The long-term stability of the human gut microbiota,” *Science*, vol. 341, no. 6141, p. 1237439, Jul. 2013.
[46] J. A. Ascensao, K. M. Wetmore, B. H. Good, A. P. Arkin, and O. Hallatschek, “Quantifying the local adaptive landscape of a nascent bacterial community,” *Nat. Commun.*, vol. 14, no. 1, p. 248, Jan. 2023.
[47] B. R. Levin, V. Perrot, and N. Walker, “Compensatory mutations, antibiotic resistance and the population genetics of adaptive evolution in bacteria,” *Genetics*, vol. 154, no. 3, pp. 985–997, Mar. 2000.
[48] F. M. Key *et al.*, “On-person adaptive evolution of Staphylococcus aureus during treatment for atopic dermatitis,” *Cell Host Microbe*, vol. 31, no. 4, pp. 593–603.e7, Apr. 2023.
[49] B. Shopsin, A. Drlica-Wagner, B. Mathema, R. P. Adhikari, B. N. Kreiswirth, and R. P. Novick, “Prevalence of agr dysfunction among colonizing Staphylococcus aureus strains,” *J. Infect. Dis.*, vol. 198, no. 8, pp. 1171–1174, Oct. 2008.
[50] H. C. Barreto, A. Sousa, and I. Gordo, “The Landscape of Adaptive Evolution of a Gut Commensal Bacteria in Aging Mice,” *Curr. Biol.*, vol. 33, no. 23, p. 5272, Dec. 2023.
[51] E. S. Snitkin *et al.*, “Genomic insights into the fate of colistin resistance and Acinetobacter baumannii during patient treatment,” *Genome Res.*, vol. 23, no. 7, pp. 1155–1162, Jul. 2013.
[52] A. Sousa, R. S. Ramiro, J. Barroso-Batista, D. Güleresi, M. Lourenço, and I. Gordo, “Recurrent Reverse Evolution Maintains Polymorphism after Strong Bottlenecks in Commensal Gut Bacteria,” *Mol. Biol. Evol.*, vol. 34, no. 11, pp. 2879–2892, Nov. 2017.
[53] A. J. Poret *et al.*, “De novo mutations mediate phenotypic switching in an opportunistic human lung pathogen,” *bioRxiv*, Feb. 2024, doi: 10.1101/2024.02.06.579193.
[54] F. Tajima, “Infinite-allele model and infinite-site model in population genetics,” *J. Genet.*, vol. 75, no. 1, pp. 27–31, Apr. 1996.
[55] J. Charlesworth and A. Eyre-Walker, “The other side of the nearly neutral theory, evidence of slightly advantageous back-mutations,” *Proc. Natl. Acad. Sci. U. S. A.*, vol. 104, no. 43, pp. 16992–16997, Oct. 2007.
[56] X. Jiang *et al.*, “Invertible promoters mediate bacterial phase variation, antibiotic resistance, and host adaptation in the gut,” *Science*, vol. 363, no. 6423, pp. 181–187, Jan. 2019.
[57] R. J. Wang, S. I. Al-Saffar, J. Rogers, and M. W. Hahn, “Human generation times across the past 250,000 years,” *Sci Adv*, vol. 9, no. 1, p. eabm7047, Jan. 2023.

[58] Z. Yang, “PAML 4: phylogenetic analysis by maximum likelihood,” *Mol. Biol. Evol.*, vol. 24, no. 8, pp. 1586–1591, Aug. 2007.
[59] B. Koskella and M. A. Brockhurst, “Bacteria-phage coevolution as a driver of ecological and evolutionary processes in microbial communities,” *FEMS Microbiol. Rev.*, vol. 38, no. 5, pp. 916–931, Sep. 2014.
[60] J. Barroso-Batista, J. Demengeot, and I. Gordo, “Adaptive immunity increases the pace and predictability of evolutionary change in commensal gut bacteria,” *Nat. Commun.*, vol. 6, p. 8945, Nov. 2015.
[61] R. N. Carmody *et al.*, “Cooking shapes the structure and function of the gut microbiome,” *Nat Microbiol*, vol. 4, no. 12, pp. 2052–2063, Dec. 2019.
[62] V. Sukhithasri, N. Nisha, L. Biswas, V. Anil Kumar, and R. Biswas, “Innate immune recognition of microbial cell wall components and microbial strategies to evade such recognitions,” *Microbiol. Res.*, vol. 168, no. 7, pp. 396–406, Aug. 2013.
[63] V. Ongenae, A. S. Mabrouk, M. Crooijmans, D. Rozen, A. Briegel, and D. Claessen, “Reversible bacteriophage resistance by shedding the bacterial cell wall,” *Open Biol.*, vol. 12, no. 6, p. 210379, Jun. 2022.
[64] T. D. Lieberman, “Detecting bacterial adaptation within individual microbiomes,” *Philos. Trans. R. Soc. Lond. B Biol. Sci.*, vol. 377, no. 1861, p. 20210243, Oct. 2022.
[65] I. Cvijović, B. H. Good, E. R. Jerison, and M. M. Desai, “Fate of a mutation in a fluctuating environment,” *Proc. Natl. Acad. Sci. U. S. A.*, vol. 112, no. 36, pp. E5021–8, Sep. 2015.
[66] A. F. Feder *et al.*, “A spatio-temporal assessment of simian/human immunodeficiency virus (SHIV) evolution reveals a highly dynamic process within the host,” *PLoS Pathog.*, vol. 13, no. 5, p. e1006358, May 2017.
[67] V. Druelle and R. A. Neher, “Reversions to consensus are positively selected in HIV-1 and bias substitution rate estimates,” *Virus Evol*, vol. 9, no. 1, p. veac118, 2023.
[68] S. Castillo-Ramírez *et al.*, “The impact of recombination on dN/dS within recently emerged bacterial clones,” *PLoS Pathog.*, vol. 7, no. 7, p. e1002129, Jul. 2011.
[69] D. W. Chen and N. R. Garud, “Rapid evolution and strain turnover in the infant gut microbiome,” *Genome Res.*, vol. 32, no. 6, pp. 1124–1136, Jun. 2022.
[70] V. S. Cooper and R. E. Lenski, “The population genetics of ecological specialization in evolving Escherichia coli populations,” *Nature*, vol. 407, no. 6805, pp. 736–739, Oct. 2000.
[71] L. Vigué and O. Tenaillon, “Predicting the effect of mutations to investigate recent events of selection across 60,472 Escherichia coli strains,” *Proc. Natl. Acad. Sci. U. S. A.*, vol. 120, no. 31, p. e2304177120, Aug. 2023.
[72] M. M. Desai and D. S. Fisher, “Beneficial mutation selection balance and the effect of linkage on positive selection,” *Genetics*, vol. 176, no. 3, pp. 1759–1798, Jul. 2007.
[73] P. J. A. Cock *et al.*, “Biopython: freely available Python tools for computational molecular biology and bioinformatics,” *Bioinformatics*, vol. 25, no. 11, pp. 1422–1423, Jun. 2009.
[74] S. Álvarez-Carretero, P. Kapli, and Z. Yang, “Beginner’s Guide on the Use of PAML to Detect Positive Selection,” *Mol. Biol. Evol.*, vol. 40, no. 4, Apr. 2023, doi: 10.1093/molbev/msad041.
[75] O. Schwengers, L. Jelonek, M. A. Dieckmann, S. Beyvers, J. Blom, and A. Goesmann, “Bakta: rapid and standardized annotation of bacterial genomes via alignment-free sequence identification,” *Microb Genom*, vol. 7, no. 11, Nov. 2021, doi: 10.1099/mgen.0.000685.
[76] C. P. Cantalapiedra, A. Hernández-Plaza, I. Letunic, P. Bork, and J. Huerta-Cepas, “eggNOG-mapper v2: Functional Annotation, Orthology Assignments, and Domain

Prediction at the Metagenomic Scale," *Mol. Biol. Evol.*, vol. 38, no. 12, pp. 5825–5829, Dec. 2021.
[77] N. Y. Yu *et al.*, "PSORTb 3.0: improved protein subcellular localization prediction with refined localization subcategories and predictive capabilities for all prokaryotes," *Bioinformatics*, vol. 26, no. 13, pp. 1608–1615, Jul. 2010.
[78] J. B. S. Haldane, "A Mathematical Theory of Natural and Artificial Selection, Part V: Selection and Mutation," *Math. Proc. Cambridge Philos. Soc.*, vol. 23, no. 7, pp. 838–844, Jul. 1927.

Acknowledgements

The authors thank three anonymous reviewers, Erik van Nimwegen, and all members of the Lieberman Lab for their thoughtful feedback on this manuscript. We also thank William Shoemaker for making the data used in this work easily accessible and his feedback on the manuscript. This work was funded by a grant from the National Institutes of Health (1DP2GM140922-01 to T.D.L.) and a fellowship for the National Sciences Foundation (to P.A.T.).

Code Availability

Code and simulation results are available at https://github.com/PaulTorrillo/Microbiome_Reversions.

Methods

Data and parameter estimation

Data was obtained from Shoemaker and Garud [21] and was initially generated by Garud & Good et al [19]. Pairwise d_N/d_S values can be found in the Github repository. The parameters are estimated by using scipy.optimize.curve_fit. The fit minimizes the RMSD of the *logarithmic* d_N/d_S. If we fit the data by minimizing just d_N/d_S on a linear scale, we get $s \approx 2.0 \times 10^{-5}$ which suggests even weaker purifying selection (Fig. S1). We analyzed the 10 species with the most data points reflecting short divergence times (d_S<0.0005), which is critical for data fit.

Basic population simulations

The majority of the computational simulations performed are built upon the idea of the Wright-Fisher Model with selection [71] that population generations can be determined from a multinomial distribution. However, we have made some changes to generalize this model for our purposes.

First, the simulations do not necessarily assume a constant population size, but rather assume the population grows via a logistic growth model with a capacity to allow for

implementation of bottlenecks. Specifically, if $P[t]$ is the population on generation t and K is the population capacity, then

$$\overline{P[t+1]} = P[t] + P[t](1 - \frac{P[t]}{K})$$

And

$$P[t+1] = Poiss(\overline{P[t+1]})$$

The population size is a Poisson random variable as we choose to determine the offspring of individual genetic classes as a Poisson random variable. We note that except for the very first few generations and after bottlenecks, the population size only has small fluctuations around a fixed capacity.

To speed the simulation up and enable simulation of very large population sizes, we implemented a variety of allele classes, rather than tracking each genotype individually. Allele classes are similar to the practice of simulating fitness classes [72] though we manage the number of unique classes via Poisson merging and splitting. We first break the total population, $P[t]$, at generation t into different classes. The number of individuals in class j on generation t will be $A_j[t]$. We have

$$P[t] = \sum_{j \geq 0} A_j[t]$$

Within class j we can store a number of variables that provide information about the genotype of members of $A_j[t]$. Specifically, we can store a number j_k that specifies the number of alleles of type k in the class j_k. Examples of potential types that could be used include deleterious allele, beneficial alleles, or alleles that resulted from a reversion. Each type of allele will be associated with a specific selective advantage s_k.We can now write a formula to calculate the absolute fitness F_j of class j

$$F_j = \prod_{k \geq 0} (1 + s_k)^{j_k}$$

From the absolute fitness F_j, we calculate the average absolute fitness of the population on generation t via

$$E[F] = \frac{\sum_{j \geq 0} F_j A_j[t]}{P[t]}$$

This allows us in turn to calculate the relative fitness of class j on generation t which will be given as

$$f_j = \frac{F_j}{E[F]}$$

Now we can calculate the expected size of class j in the next generation with

$$A_j[t+1] = f_j(A_j[t] + A_j[t](1 - \frac{P[t]}{K}))$$

Note that

$$P[t+1] = \sum_{j \geq 0} A_j[t+1] = \sum_{j \geq 0} f_j(A_j[t] + A_j[t](1 - \frac{P[t]}{K})) =$$

$$\sum_{j \geq 0} \frac{F_j}{E[F]}(A_j[t] + A_j[t](1 - \frac{P[t]}{K})) = P[t] + P[t](1 - \frac{P[t]}{K})$$

This allows us to use a logistic model of growth to represent population size rather than being constrained to fixing it. This is useful for simulating bottlenecks. However, the simulation as laid out does not take into account genetic drift through random fluctuations. To do this, we rewrite the above equations to be

$$A_j[t+1] = Poiss(f_j(A_j[t] + A_j[t](1 - \frac{P[t]}{K})))$$

Which also implies

$$P[t+1] = Poiss(P[t] + P[t](1 - \frac{P[t]}{K}))$$

Note that this simulation still has equivalent dynamics of the frequencies of classes as a Wright-Fisher Model with selection in the case of a fixed population size. This is because of the ability to split Poisson processes i.e.

$$Pr(A_j[t+1] = X \mid P[t+1]) = Pr(Bin(P[t+1], \frac{f_j A_j[t+1]}{P[t]}) = X)$$

Mutations are added in every generation depending on the mutation rate. Only single mutants are generated per generation and an organism cannot get more than one mutation per generation. The number of new mutants are determined by the binomial distribution. New mutants are added then to their appropriate class j. For example, if a deleterious mutation is gained in a class with 10 deleterious alleles (and nothing else), this new mutant will increase the population size of the class with 11 deleterious alleles (and nothing else) while decreasing the population size of the class with 10 deleterious alleles (and nothing else).

By grouping individuals in classes rather than by genotype, computational cost can be greatly cut down on. Grouping individuals does not affect the dynamics of the simulation because the merging of Poisson processes is still Poisson. The downside to this approach is information loss, however in our situation we have already defined the classes to contain all the

information we are interested in. For example, we require that when a mutation occurs, the new allele must come from a current allele (i.e. instead of a deleterious mutation take an organism from a class with 1000 neutral alleles to a class with 1000 neutral alleles and 1 deleterious allele, we go to a class with 999 neutral alleles and 1 deleterious allele). Furthermore, a deleterious allele can be converted to another class of alleles to keep track of reversions.

Stop codon enrichment in Zhao & Lieberman et al dataset

Table S7 in Zhao & Lieberman et al [24] provides an excel sheet detailing all observed mutations. There were 325 observed nonsynonymous mutations of which 28 were stop codons. Under a null model there are 415 possible permutations of initial codon and codon one mutation (see code repository) away that result in a nonsynonymous substitution of which 23 lead to a stop codon. Assuming no preference for specific mutation or initial codon, we would expect roughly 18 stop codons in this data. Under a null binomial distribution, the p value for obtaining 28 or more is 0.015.

Reversion simulations

We simulated gut bacterial populations using a modified Wright-Fisher model (see **Basic population simulations**) to monitor mutation acquisition over time compared to an ancestor. Environmental changes occur with a probability of $\frac{n_{loci}}{\tau_{flip}}$ per generation, triggering an average of one selective pressure per environmental change, modeled by a Poisson distribution. Population bottlenecks to 10 individuals occur independently of environmental changes with a probability of 10^{-4} per generation (see Fig. S10 for an alternative in which bottlenecks and environmental change are correlated).

Adaptive mutations were categorized into two types: forward and reverse. We calculated actual d_N/d_S using the sum of these mutations and observed d_N/d_S using their difference (plus asymptomatic d_N/d_S). When releasing beneficial mutations, their classification as forward or reverse is based on the balance of previously released mutations: the probability of a mutation being a reverse adaptation is the difference between the forward mutations previously released (m_F) and reverse mutations previously released (m_R) divided by the number of loci (i.e. $\frac{m_F - m_R}{n_{loci}}$). Given the specificity needed for true reversions, their likelihood is set at one-fifth the rate of nonsynonymous mutations (4.5×10^{-10}) per generation per cell), while forward mutations are set at a rate 5 times higher than the nonsynonymous mutation rate (25x the reversion rate; 1.1×10^{-8} per generation per cell). All beneficial mutations had a selective advantage of s_{ben}=0.03 (for forward or reverse).

Each adaptive mutation was treated as occupying a unique codon in the core genome, simplifying computations. This assumes that the ancestral allele at a given locus has been purged before the next environmental change affecting that locus; as theory suggests that a beneficial mutation takes 768 generations to fix (SI Text 2.2), compared to 46,200 generations for pressure shifts at any locus we believe this assumption is reasonable. To confirm this theory still holds in

785 the presence of bottlenecks and clonal interference, we tracked the average number of beneficial
786 mutations in the population relative to the number of mutations available at any generation in
787 simulations; we found only 2% deviation between the average and expected total beneficial
788 mutations over 2×10^6 generations. Throughout the simulation, deleterious mutations occur at a
789 rate of 1.01×10^{-3} mutations per genome per generation with a selective disadvantage of s =
790 0.003 and could be reverted (similar to a release of a beneficial mutation as above, but with a
791 lower s_{ben}).
792
793 **Testing standard d_N/d_S software**
794 We simulated gene sequences with selective pressures acting at specific sites for Fig. 4b.
795 For each genomic distance investigated (every 500,000 bacterial generations), we ran 10
796 simulations as described below, with each simulation resulting in 10 sequences derived from a
797 branching process. In the permanent adaptations simulation (blue), adaptive mutations in the
798 phylogeny are acquired simply and permanently. In the transient adaptations simulation (red),
799 only more recent mutations in the same phylogeny will be visible while older mutations are
800 obscured by reversion. Both sets of sequences were then fed to PAML v4.8 [58] for estimation of
801 d_N/d_S values. PAML uses maximum likelihood analysis to estimate the rate of substitution that
802 best explains a given phylogenetic tree.
803 For each simulation, we generated a random 1,500 bp open reading frame, and designated
804 10% of codons as neutral, 10% under positive selection, and 80% under purifying selection. We
805 introduced mutations and branches across several cycles, with each cycle representing 100,000
806 generations. Each cycle, we assigned mutations at random accordingly to the following
807 probabilities: 67.5% that a nonsynonymous mutation occurred at a codon under positive
808 selection, 12.5% for synonymous mutation at any codon, 3.75% for nonsynonymous mutation at
809 a non-selected site (neutral), and 16.25% for no mutation. These values were selected to give a
810 d_N/d_S of around 2 and to match the general ratios in the reversion model.
811 Two phylogenies were constructed from each simulation: both received identical
812 mutations, but they differed in how nonsynonymous mutations at selective codon sites were
813 visible at the end of the simulation. In the transient adaptations version of the phylogeny,
814 nonsynonymous mutations at selective codon sites were reverted at the end of simulation, except
815 those that occurred within the last 500,000 generations. Reverted sites were converted to a
816 synonymous substitutions at a frequency based on the codon table (assuming equal probability of
817 all nucleotide mutations). Both versions of the sequences underwent multiple sequence
818 alignment and neighbor-joining tree construction (Biopython [73]). We calculated treewide d_N/d_S
819 ratios using PAML v4.8's codeML feature [74], employing the M2a model to analyze
820 site-specific selection.
821
822 **Closeness to stop codons**
823 To evaluate possible enrichment for stop codon adjacency, we focused on TTA and TCA
824 codons. TTA and TCA are ideal to measure likelihood of nonsense mutations because each has

two point mutations that yield a stop codon, unlike the five other redundant codons encoding for the same amino acids (for both leucine and serine, one codon is singly stop codon adjacent and the last four are not stop codon adjacent). In *Bacteroides fragilis,* these codons have a codon usage rate of 13% for leucine and 14% for serine.

We annotated the reference genome NCTC_9343 with Bakta v1.9 [75] and obtained COG (Clusters of Orthologous Genes) categories for each gene using eggNOG v5.0 [76]. Genes that did not have a functional COG category (35%) were removed. To control for unusual outlier genes skewing results, only the 15 COG groups that had at least 50 genes were considered for enrichment analyses. For each COG category, we calculated a null codon usage proportion based on the proportion of leucine and serine codons, and compared this to the actual proportion using a one-proportion Z test. To address the fact that genes in the same functional category but localized to different parts of the cell may be under different selective pressure, we analyzed cellular location classifications from PSORTb v3.02 [77] and categorized genes by the combination of function and localization. We analyzed the 15 function-location combinations with more than 50 genes. After identifying those categories that were significantly enriched, we cross referenced which categories genes shown do be under adaptive within-person evolution in a previous study of *B. fragilis* within-person evolution were in [24]. Of the 16 genes reported in that paper, 8 were assigned a functional COG category/cellular location and in the reference genome (NCTC_9343). Four of these were in inorganic ion transport and metabolism, a significant enrichment ($p = 1.22 \times 10^{-4}$; binomial test).

Supporting Information

1.1 d_N/d_S theory

The following is meant to provide a more indepth walkthrough of how one can build up and interpret the purifying selection model and its effect of time dependence on d_N/d_S. In an effort to be accessible to a wide audience and self contained, we have included enough detail that for most sections should be followable with basic knowledge of calculus.

Assume an infinite population of organisms. Consider the existence of m classes of nonsynonymous mutations. The number of mutations of the ith class in the population is represented by the variable $\overline{N}_i$. Each class $\overline{N}_i$ has an associated mutation rate U_i (mutations per genome per generation per unit time) and an associated selective disadvantage s_i (mutation purification per unit time). In the purifying selection model we assume that $s_0 = 0$ and $s_{i>0} > 0$. We assume that both the mutation rate and the selective disadvantage of each class remain constant throughout time. We assume this is the global population and hence no migration. We then have

$$d\overline{N}_i = U_i dt - s_i \overline{N}_i dt \quad \text{(S1)}$$

Assuming $i > 0$, we can integrate

$$\frac{dN_i}{U_i - s_i \overline{N}_i} = dt$$

Using u substitution, we let $u = \mu_i - s_i \overline{N}_i$ so that $\frac{du}{d\overline{N}_i} = - s_i$ which implies $d\overline{N}_i = \frac{du}{-s_i}$ so that

$$\frac{du}{-s_i u} = dt$$

Integrating both sides we get

$$\frac{-ln(u)}{s_i} = t + C$$

Where C is the constant of integration. Continuing we have

$$u = e^{-s_i t - s_i C}$$

$$\mu_i - s_i \overline{N}_i = e^{-s_i t - s_i C}$$

$$\overline{N}_i = \frac{\mu_i}{s_i} - \frac{e^{-s_i t - s_i C}}{s_i}$$

We can remove the constant of integration and instead replace it by initial condition $\overline{N}_i(0)$

$$\overline{N}_i(0) = \frac{U_i}{s_i} - \frac{e^{-s_i C}}{s_i}$$

So then we have that

$$C = \frac{ln(U_i - s_i \overline{N}_i(0))}{-s_i}$$

So that we get

$$\overline{N}_i = \frac{U_i}{s_i}(1 - e^{-s_i t}) + \overline{N}_i(0) e^{-s_i t}$$

Since $\overline{N}_i(0)$ should occur at a homogenous population that is the most recent common ancestor of the individuals in the population we are observing, we assume $\overline{N}_i(0)$=0 so we have

$$\overline{N}_i = \frac{U_i}{s_i}(1 - e^{-s_i t}) \quad \text{(S2)}$$

If $i = 0$, we have

$$\overline{N}_0 = U_0 t$$

We also assume that there are synonymous mutations $\overline{S}$ which are neutral and occur with new mutations per unit time U_S so that

$$\overline{S} = U_S t$$

So if we want to find $\overline{N}$ (the total number of nonsynonymous mutations), that will be given by

$$\overline{N} = U_0 t + \sum_{i \geq 1} \frac{U_i}{s_i}(1 - e^{-s_i t}) \quad \text{(S3)}$$

Now observe the following with G as the number of base paris in the core genome, then $d_N = 2\overline{N}/(G \times 3/4)$ and $d_S = 2\overline{S}/(G \times 1/4)$. The two comes from the fact that there are two diverged lineages when calculating d_N/d_S .

$$\frac{d_N}{d_S} = \frac{1}{3}\frac{\overline{N}/G}{\overline{S}/G} = \frac{U_0 t + \sum_{i \geq 1} \frac{U_i}{s_i}(1 - e^{-s_i t})}{U_S t} = \frac{1}{3}\left(\frac{U_0}{U_S} + \sum_{i \geq 1} \frac{U_i/U_S}{s_i t}(1 - e^{-s_i t})\right) \quad \text{(S4)}$$

The ⅓ is for normalization. While the above form is easier to analyze in terms of actual time, it should also be noted that data is given in terms of d_S rather than t so the following equivalent form can also be helpful when discussing fitting of the timescale dependence of d_N/d_S

$$\frac{d_N}{d_S} = \frac{1}{3}\left(\frac{U_0}{U_S} + \sum_{i \geq 1} \frac{2U_i}{G s_i d_S}(1 - e^{-\frac{G s_i}{2U_S} d_S})\right)$$

Furthermore, we can rewrite $U_i = 3\alpha_i U_S$ so that we have

$$\frac{d_N}{d_S} = \alpha_0 + \sum_{i \geq 1} \frac{2\alpha_i U_S}{G s_i d_S}(1 - e^{-\frac{G s_i}{2U_S} d_S})$$

Note α_0 is equivalent to α in the main text. Next we can simply rewrite $\beta_i = \frac{G s_i}{2U_S}$ so that we have

$$\frac{d_N}{d_S} = \alpha_0 + \sum_{i\geq 1} \frac{\alpha_i}{\beta_i d_S}(1 - e^{-\beta_i d_S}) \qquad \text{(S5)}$$

To begin analyzing (S5), we consider the asymptotic behavior. First, we note that

$$\lim_{dS \to +\infty} \alpha_0 + \sum_{i\geq 1} \frac{\alpha_i}{\beta_i d_S}(1 - e^{-\beta_i d_S}) = \alpha_0 = \frac{U_0}{U_S} \qquad \text{(S6)}$$

For initial behavior, we can use L'Hopital's Rule

$$\lim_{dS \to +0} \alpha_0 + \sum_{i\geq 1} \frac{\alpha_i}{\beta_i dS}(1 - e^{-\beta_i dS}) = \alpha_0 + \sum_{i\geq 1} \alpha_i = \frac{U_0 + \sum_{i\geq 1} U_i}{U_S} \qquad \text{(S7)}$$

Finally, we are interested in when d_N/d_S ends up being in between these initial and final values. Each class i has a different midpoint at which its contribution to d_N/d_S is a half. In mathematical terms, this can be summarized as

$$\frac{\alpha_i}{2} = \frac{\alpha_i}{\beta_i d_S}(1 - e^{-\beta_i d_S})$$

Which implies

$$\frac{\beta_i d_S}{2} = (1 - e^{-\beta_i d_S})$$

Thus, we see that for any class of mutation, $\frac{1}{s_i}$ will determine the midpoint (assuming some constant U_S and G). We can then imagine the curve as similar to a step function where the location of each step is determined by the corresponding $\frac{1}{s_i}$ and how far the function steps down will be determined by the size of the mutation rate U_i. Finally, we can surmise that the average step down occurs at approximately the harmonic average

$$s^{-1} = \sum_{i\geq 1} \frac{U_i}{U_N s_i}$$

Where $U_N = \sum_{i\geq 1} U_i$, which represent the total nonneutral nonsynonymous mutation rate.

Taking this all into account, here is exactly what is being fit in the d_N/d_S curve. We are fitting the equation

$$\frac{d_N}{d_S} = \alpha + \frac{1-\alpha}{\beta d_S}(1 - e^{-\beta d_S}) \qquad \text{(S8)}$$

α is the fraction of nonsynonymous mutations that are neutral. Now β is a compound parameter and we are able to fit $\beta = \frac{Gs}{2U_S}$ which is essentially half of the harmonic average of selective disadvantages in ratio with the synonymous mutation rate per site per generation. Now we can estimate the synonymous mutation per site per generation with the following

$$10^{-9}\ \frac{mutations}{base\ pair \times generation} \times 3\frac{base\ pairs}{site} \times \frac{1}{4}\frac{synonymous\ mutation}{mutations} = \frac{3}{4} \times 10^{-9} \times \frac{synonymous\ mutations}{site \times generation}$$

Thus we are truly fitting:

$$\frac{d_N}{d_S} = \alpha + \frac{\frac{3}{4}\times(1-\alpha)\times 10^{-9}}{2sd_S}\left(1 - e^{-\frac{s}{\frac{3}{2}\times 10^{-9}}d_S}\right) \quad \text{(S9)}$$

1.2 Mutation accumulation

In order to analyze genetic drift and Muller's Ratchet [26] [40], we will provide a brief overview of the approach well suited for our work. For any nonsynonymous mutation class N_i with $i > 0$, we can track the size of a population with 0 mutations of class N_i, denoted by variable W_i, via

$$dW_i = s_i\overline{N}_i(t)W_i dt - U_i W_i dt \quad \text{(S10)}$$

Here $\overline{N}_i(t)$ is the average number of mutations of class $\overline{N}_i$ in the population and $s_i\overline{N}_i(t)W_i$ is equivalent to mean fitness. This equation reflects how every unit time, the mutation free class should increase by its selective advantage relative to the population though also lose members of the population to the mutation rate.

If we substitute in $\overline{N}_i(t)$ we get

$$dW_i = s_i\frac{U_i}{s_i}\left(1 - e^{-s_i t}\right)dt - U_i W_i dt$$

$$dW_i = U_i\left(1 - e^{-s_i t}\right)W_i dt - U_i W_i dt$$

$$dW_i = -U_i e^{-s_i t} W_i dt$$

So then

$$ln(W_i) = \frac{U_i}{s_i}e^{-s_i t} + C$$

Assuming that W_i at time 0 is given by W_0 (representing the initial population size which under our assumptions is always free of mutations and hence wild type) then

$$ln(W_0) = \frac{U_i}{s_i} + C$$

$$C = ln(W_0) - \frac{U_i}{s_i}$$

$$W_i(t) = W_0 e^{-\frac{U_i(1-e^{-s_i t})}{s_i}} \quad \text{(S11)}$$

We see that if we set $W_0 = 1$, then everything can be given in terms of frequencies within the population. Asymptotically, we have that

$$\lim_{t \to \infty} W_0 e^{-\frac{U_i(1-e^{-s_i t})}{s_i}} = W_0 e^{-\frac{U_i}{s_i}} \quad \text{(S12)}$$

Importantly, we also note the following: Let W be the frequency of the wild type (mutation free class) and $W_0 = 1$. Then

$$W(t) = \prod_{i>0} W_i(t) = e^{-\sum_{i>0} \frac{U_i(1-e^{-s_i t})}{s_i}} \quad \text{(S13)}$$

Which implies

$$\lim_{t \to \infty} e^{-\sum_{i>0} \frac{U_i(1-e^{-s_i t})}{s_i}} = e^{-\sum_{i>0} \frac{U_i}{s_i}} = e^{-\frac{U_N}{s}} \quad \text{(S14)}$$

Once again using

$$U_N = \sum_{i \geq 1} U_i$$

And

$$s^{-1} = \sum_{i \geq 1} \frac{U_i}{U_N s_i}$$

Furthermore, the average time for the frequency in the population without mutations of class i to reach one half of the logarithm of the asymptotic frequency is the same when using the above simplifications. In other words, the difference in how much and how fast the wild type is lost should not depend too heavily on the distribution of selective coefficients.

Finally, we can predict if the least loaded class will actually be lost to drift. We can form this prediction via the following. We make the assumption that if the least loaded class W drops below its steady state frequency, $e^{-\frac{U_N}{s}}$, it will have advantage s every generation. If the least loaded class has advantage s then it has a $2s$ probability of extinction (see SI Text 2.1). Hence, if we expect there to be $N_e e^{-\frac{U_N}{s}}$ individuals, we can estimate that mutation accumulation will occur when

$$2sN_e e^{-\frac{U_N}{s}} << 1 \text{ (S15).}$$

2.1. Extinction and fixation probability

Here we will derive how the fixation probability of a mutation with selective advantage s_{ben} is approximately $2s_{ben}$. This is a standard result that can be found in classic population genetics textbooks. It is usually derived via differential equations but can also be obtained more classically from the study of branching processes [78] which we will use here. First, we assume that individuals reproduce via a Galton-Watson branching process with mean $1+s_{ben}$. We also assume there are no other mutations in the population that can interfere with fixation or extinction. A fundamental result from the study of branching processes is that the extinction probability is given by the smallest nonnegative root of the branching processes corresponding probability generating function, f(z). Being a Galton-Watson branching process, the probability generating function is the the probability generating function of a Poisson process so

$$f(z) = e^{(1+s_{ben})(1-z)}$$

Thus we need to find the smallest nonnegative solution, z, to

$$e^{(1+s_{ben})(1-z)} - z = 0$$

We can use a second order Taylor approximation to approximate the exponential so we have

$$1 + (1 + s_{ben})(z - 1) + \frac{((1+s_{ben})(z-1))^2}{2} - z = 0$$

Which has a smallest nonnegative solution of

$$z = \frac{s_{ben}^2+1}{(s_{ben}+1)^2}$$

If s_{ben} is small then we have

$$z \approx \frac{1}{1+2s_{ben}}$$

Which we can further approximate by doing

$$z \approx \frac{1}{1+2s_{ben}} \frac{1-2s_{ben}}{1-2s_{ben}} \approx 1 - 2s_{ben} \quad \text{(S16)}$$

If $1 - 2s_{ben}$ is the extinction probability then the fixation probability will be $2s_{ben}$.

2.2. Likelihood of reversion

We calculate time for mutations to occur and fix in the population for demonstration in Fig. 3b. For the sake of simplicity, we consider the weak-mutation strong selection regime (no clonal interference) in our theory but do include such dynamics in our simulations. Regardless, clonal interference will only minorly change the frequency of a revertant with high s_{ben} in the population, as multiple backgrounds will find the same reversion when N_e is sufficiently high. The expected time to fixation given a mutation with selective coefficient s_{ben} is estimated using

$$(1 + s_{ben})^t = N_e$$

Where N_e is the census population size. The above implies

$$tln(1 + s_{ben}) = ln(N_e)$$

And if s_{ben} is small then we have

$$t = \frac{ln(N_e)}{s_{ben}} \quad \text{(S17)}$$

Now we need to know the expected time for a fixing mutant to arise. First, we want the probability the mutation arises and fixes which will be given by

$$1 - (1 - 2s_{ben}U_{ben})^{N_e} \approx 2N_e s_{ben} U_{ben}$$

Which implies the expected time to arisal is approximately

$$\frac{1}{2N_e s_{ben} U_{ben}} \quad \text{(S18)}$$

So therefore, in the absence of clonal interference, the time for reversion to fix in the population depends more on the time for it to fix over time than the time for the reversion to arise (and is therefore less dependent on the mutation rate) if

$$\frac{1}{2N_e s_{ben} U_{ben}} < \frac{ln(N_e)}{s_{ben}}$$

Or alternatively written as

$$1 < 2N_e U_{ben} ln(N_e) \quad \text{(S19)}$$

Finally, note that the expected time to fixation is given by

$$\frac{1}{2N_e s_{ben} U_{ben}} + \frac{ln(N_e)}{s_{ben}} \quad \text{(S20).}$$

The second term can be larger because of bottlenecks and clonal interference.

3.1 Reversion model with fluctuating loci

The reversion model can be derived in the following way. First, one can rewrite equation (2) as a generic negative feedback model in which mutations emerge and are purged from the population at a rate proportional to how many mutations have accumulated:

$$dN_{transient} = R_{in} dt - P_{out} N_{transient} dt \quad \text{(S21)}$$

In this formulation, R_{in} is simply the rate of accumulation of transient nonneutral nonsynonymous mutations per genome per unit time and P_{out} is the loss rate of these mutations per unit time.

From this more general form, we can develop the reversion model. Similar to the original purifying selection model, it is possible to assume a variety of classes of mutations but for simplicity we only assume 1. If we make the following definitions for

$$R_{in} = \frac{n_{loci}}{\tau_{flip}}$$

$$P_{out} = \frac{2}{\tau_{flip}}$$

we can link Equation (S21) to a fluctuating loci model via

$$\frac{d\overline{N}_{transient}}{dt} = R_{in} - P_{out}\overline{N}_{transient} = \frac{n_{loci}}{\tau_{flip}} - \frac{2}{\tau_{flip}}\overline{N}_{transient}$$

$$= \frac{1}{\tau_{flip}}(n_{loci} - \overline{N}_{transient}) - \frac{1}{\tau_{flip}}\overline{N}_{transient} \quad \text{(S22)}$$

Here τ_{flip} representing the average number of generations it takes for a *given* selective pressure on a loci to switch direction, and n_{loci}, the number of loci under fluctuating selective pressures. S22 can be more directly linked to a fluctuating loci model as we see the rate of nonsynonymous mutations in is proportional to $n_{loci} - \overline{N}_{transient}$ (the number of loci unmutated) and the rate out is proportional to $\overline{N}_{transient}$ the number of loci mutated.

Solving similar to the purifying selection model we have

$$\overline{N}_{transient}(t) = \frac{n_{loci}}{2}(1 - e^{-\frac{2t}{\tau_{flip}}}) \qquad \text{(S23)}$$

This can then be used to obtain d_N/d_S

$$\frac{d_N}{d_S} = \frac{1}{3}\left(\frac{U_0}{U_S} + \frac{n_{loci}}{2U_S t}(1 - e^{-\frac{2t}{\tau_{flip}}})\right)$$

Or equivalently

$$\frac{d_N}{d_S} = \frac{1}{3}\left(\frac{U_0}{U_S} + \frac{n_{loci}}{GdS}(1 - e^{-\frac{Gd_S}{U_S\tau_{flip}}})\right)$$

If we set $\alpha = \frac{U_0}{3U_S}$, $\beta = \frac{G}{U_S\tau_{flip}}$, and $\gamma = \frac{n_{loci}}{3U_S\tau_{flip}}$ so that

$$\frac{d_N}{d_S} = \alpha + \frac{\gamma}{\beta dS}(1 - e^{-\beta d_S}) \qquad \text{(S24)}$$

Which is equivalent to equation S9 with one more free parameter.

3.2 Effect of compensatory mutations

We can further extend the theory to include compensatory mutations through calculating the expected value of $N_{transient}$ as a Markov chain. First, let v be the state vector for a loci under selection where the index of each row corresponds to the number of observed mutations currently at that loci and A be the corresponding stochastic matrix with rows i and columns j. First, we need to consider the probability the state does not change on a given generation (i.e. the diagonal of A). This will be $\frac{1}{\tau_{flip}}$. For every element on the diagonal of A we thus have $A_{i=j} = 1 - \frac{1}{\tau_{flip}}$.

Supposing there is a state change, let us define p as the probability there is an increase in observed mutations (a forward or compensatory mutation) and $1 - p$, the probability there is a decrease in observed mutations (a reversion). Then, $A_{j=i-1} = \frac{1}{\tau_{flip}}p$ and $A_{j=i+1} = \frac{1}{\tau_{flip}}(1 - p)$ (with the exception of $A_{i=1,\, j=0} = \frac{1}{\tau_{flip}}$). Finally, with Δt being the number of time steps and assuming $v_0 = 1$ and $v_{i>0} = 0$ then

$$\overline{N}_{transient}(\Delta t) = n_{loci}\sum_{i\geq 0}(A^{\Delta t}v)_i \cdot i \qquad \text{(S25)}$$

If $p > 1 - p$, compensatory mutations are gained at a linear rate and the compensatory mutation rate will factor into the asymptotic d_N/d_S value. Conversely, if $p < 1 - p$, the number of compensatory mutations is almost surely finite by the central limit theorem and hence will not factor into the asymptotic d_N/d_S. Finally, if $p = 1 - p$, this is the classic elementary random walk well known to deviate from the origin with $O(\sqrt{n})$. Interestingly, this is also sublinear and will not factor into asymptotic d_N/d_S.

SI Figures

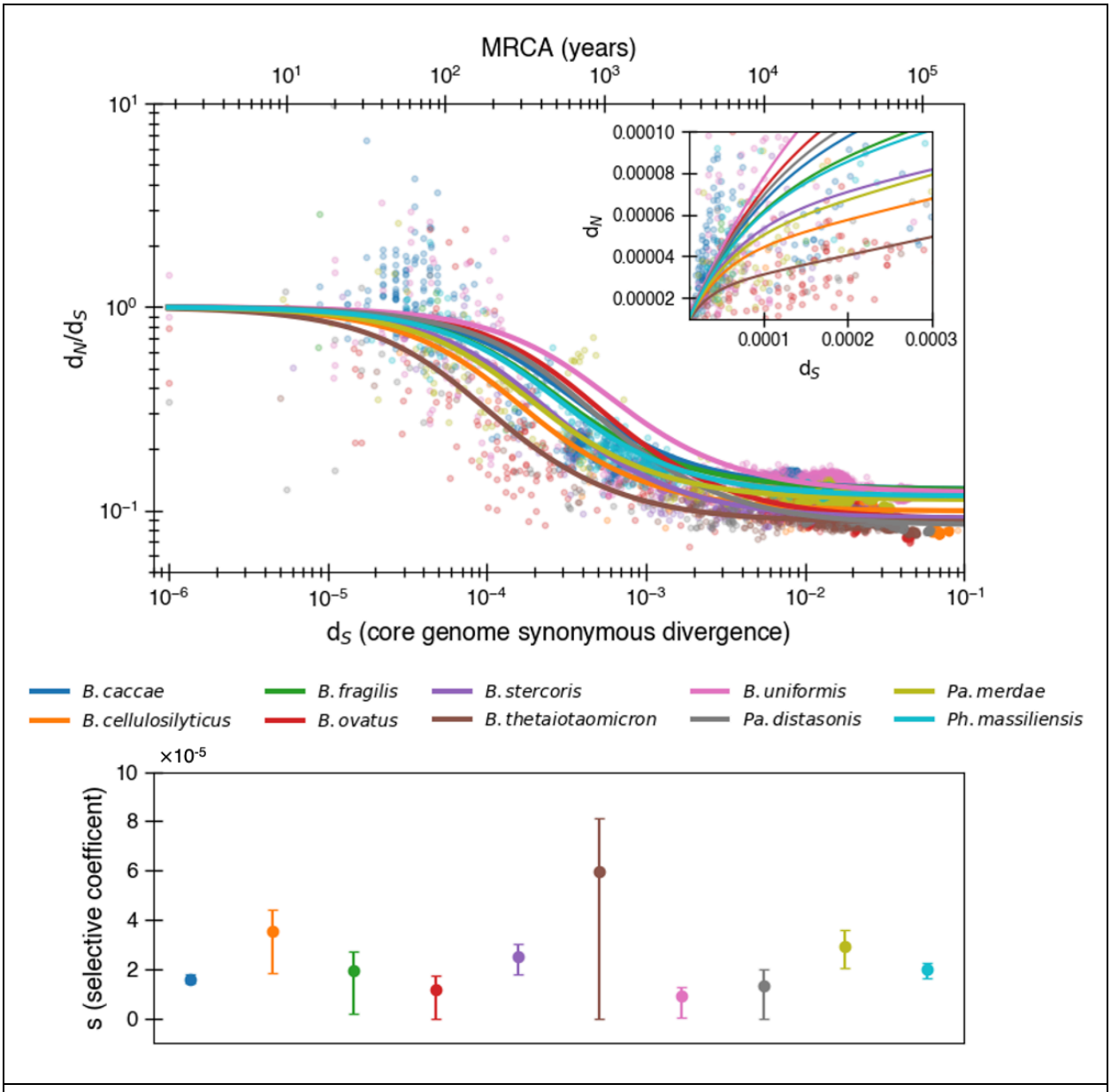

Figure S1: Purifying selection model predicts even weaker purifying selection when fitting to non logarithmic d_N/d_S. Equivalent to main text Fig. 1 except fit is determined by minimizing variance in d_N/d_S rather

than logarithmic d_N/d_S. In this fit, *s* values tend to be even smaller with a median of 2.0×10^{-5}. The median R^2=0.64 (range 0.07-0.88).

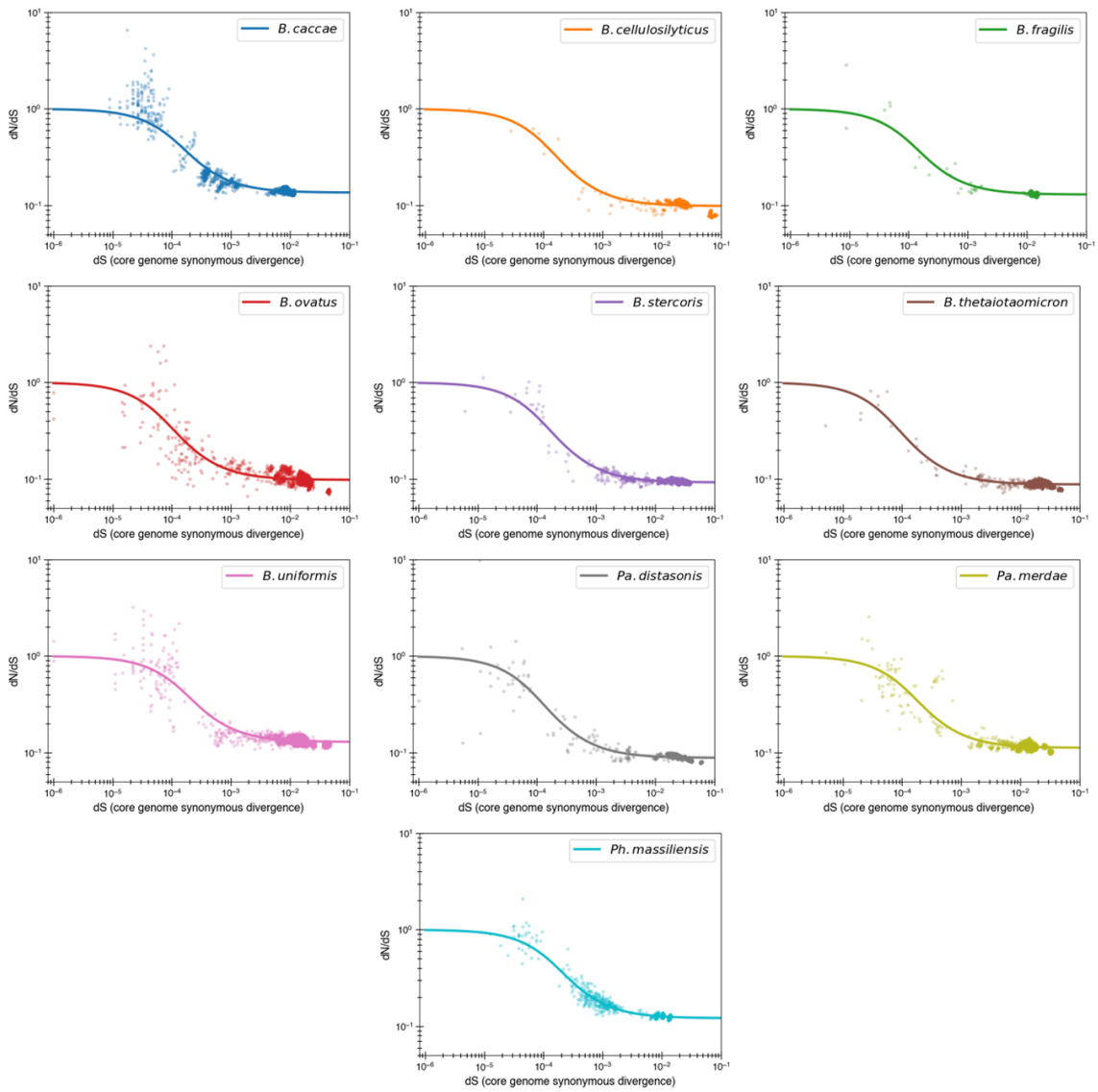

Figure S2: Purifying selection model fits by individual species. Content of Fig. 1a with each species given its own panel. One species of note is *B. caccae*, which appears to have substantial initial d_N/d_S values above 1, at odds with a purifying selection model. Fits for *s*, with uncertainty, are given in Fig. 1b.

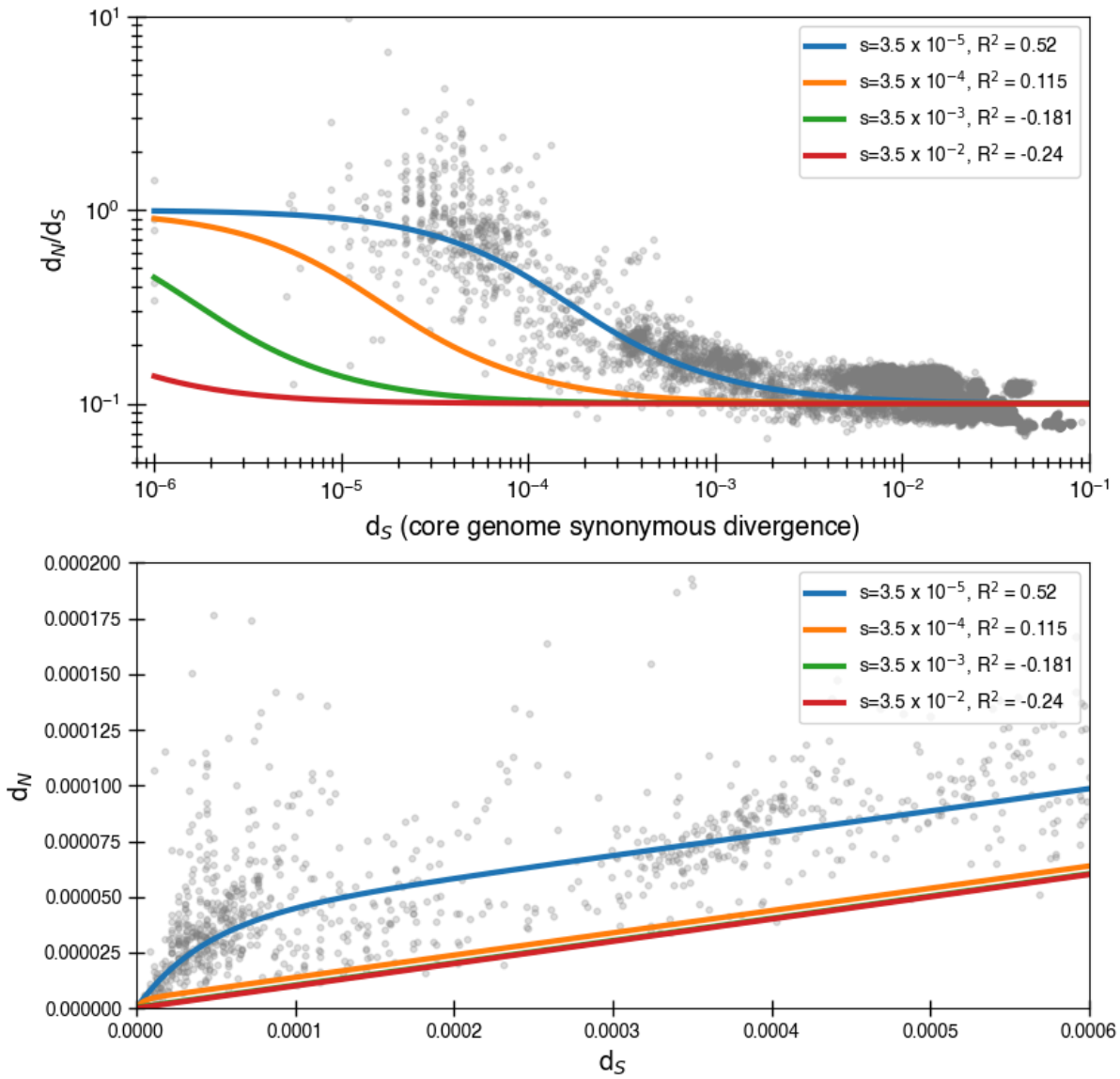

Figure S3. Larger selective coefficients rapidly lose explanatory power. Here we use equation (4) to once again fit the data. We still use $\alpha = 0.1$ but use alternate values of s. We see that significantly larger, though still relatively small, levels of purifying selection have essentially no ability to explain the data. R^2 is for minimizing the logarithmic variance.

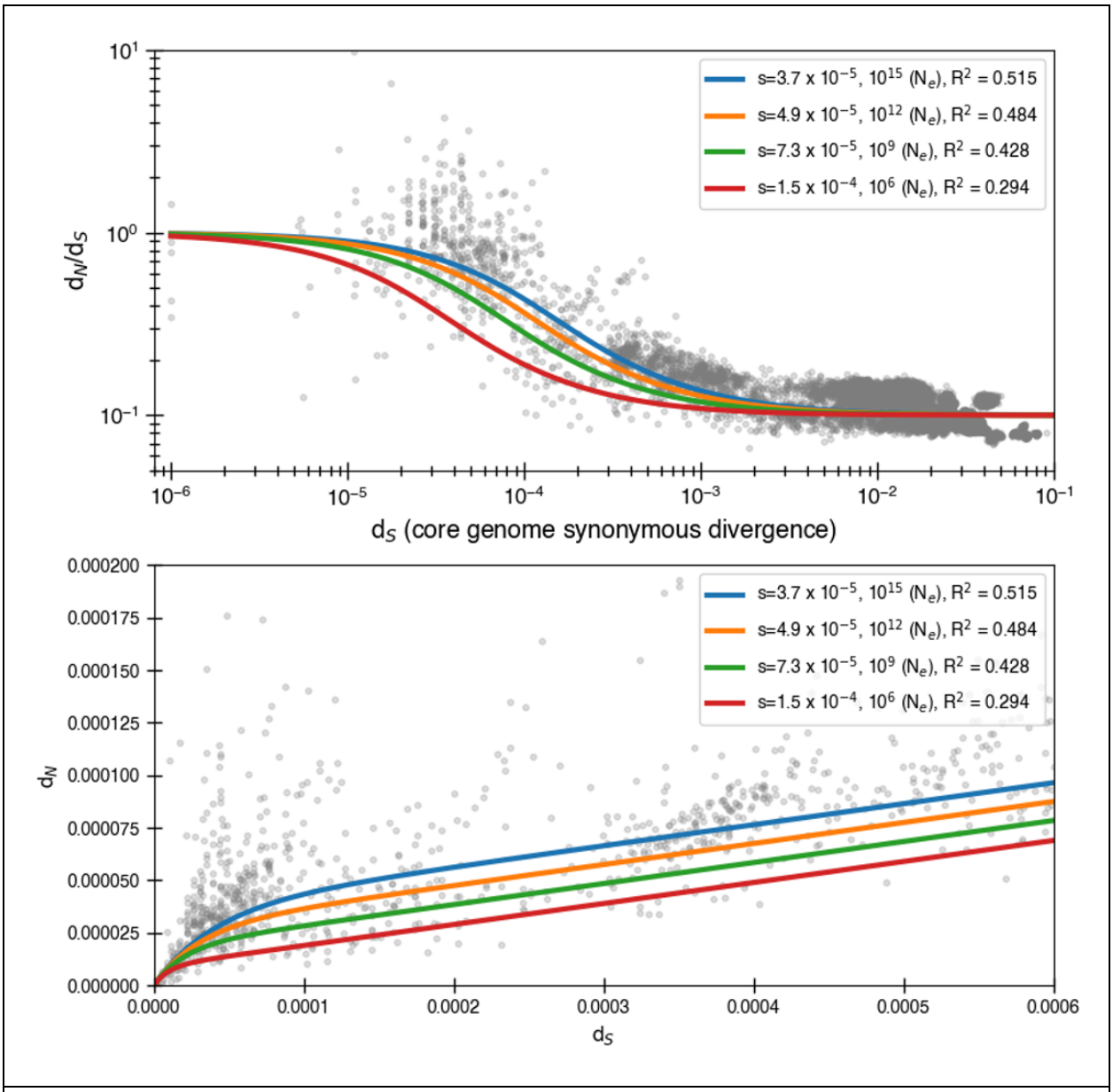

Figure S4: **Larger selective coefficients that can prevent mutation accumulation in simulations lead to less optimal data fit.** We first calculate the smallest possible *s* values (as estimated from inequality (5)) that will not lead to mutation accumulation for a given effective population size and the corresponding fits. The core genome size is assumed to be 1,500,000 nucleotides. Once again we use equation (4) to fit the data and use $\alpha = 0.1$.

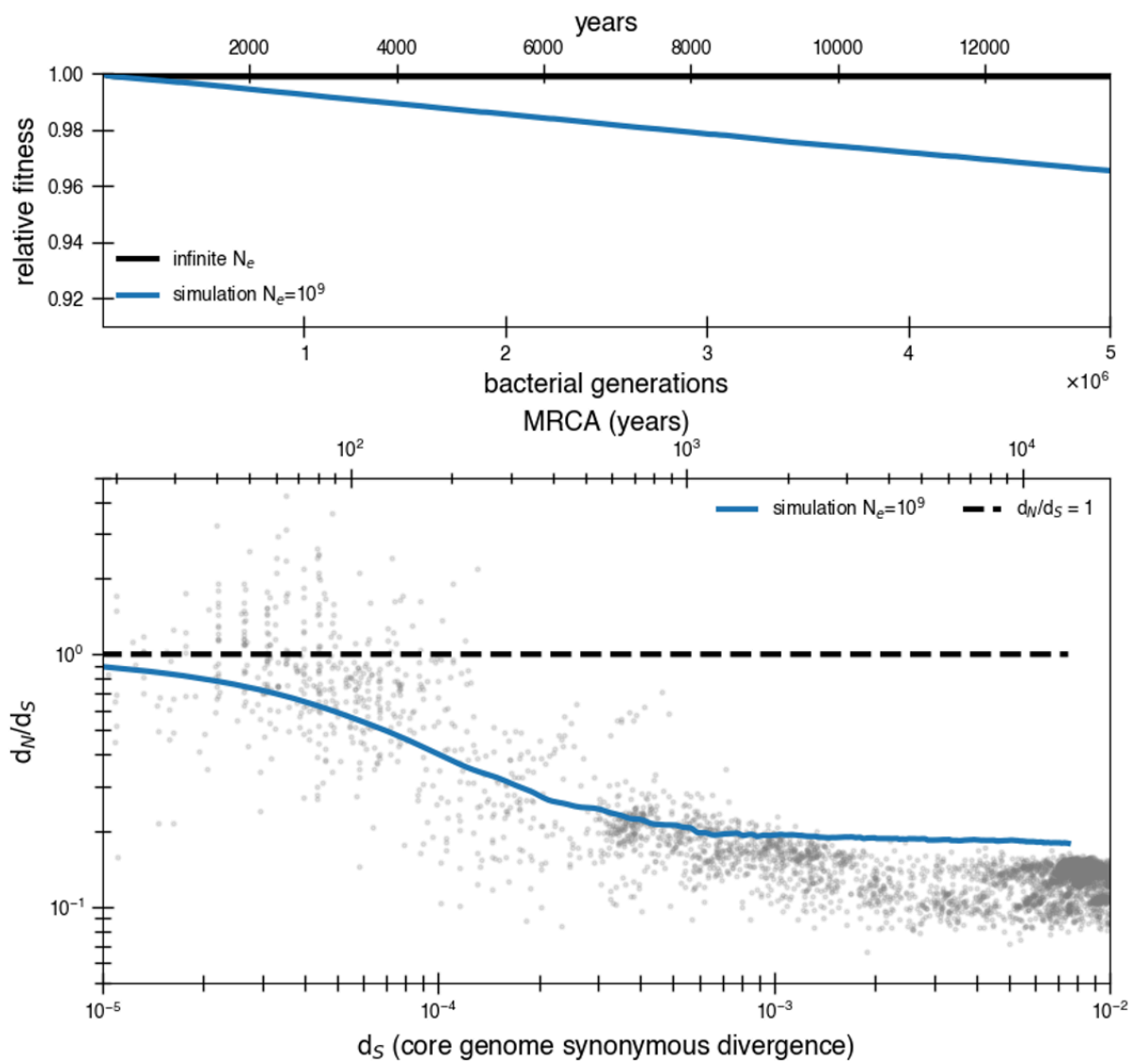

Figure S5: Even assuming all mutations are deleterious suggests a higher asymptotic d_N/d_S. A purifying selection simulation as in Fig. 2**,** except all mutations are assumed to be weakly deleterious ($s = 3.5 \times 10^{-5}$) rather than just 90%. In other words, rather than the standard deleterious mutation rate of 1.01×10^{-3} mutations per genome per generation, the mutation rate is now 1.13×10^{-3} mutations per genome per generation. With an effective population size of 10^9, mutations still occur so quickly as to raise the asymptote above the data. Furthermore, all of these mutations contributing to the asymptotic d_N/d_S are deleterious rather than neutral, furthering the problem of Muller's ratchet.

1196

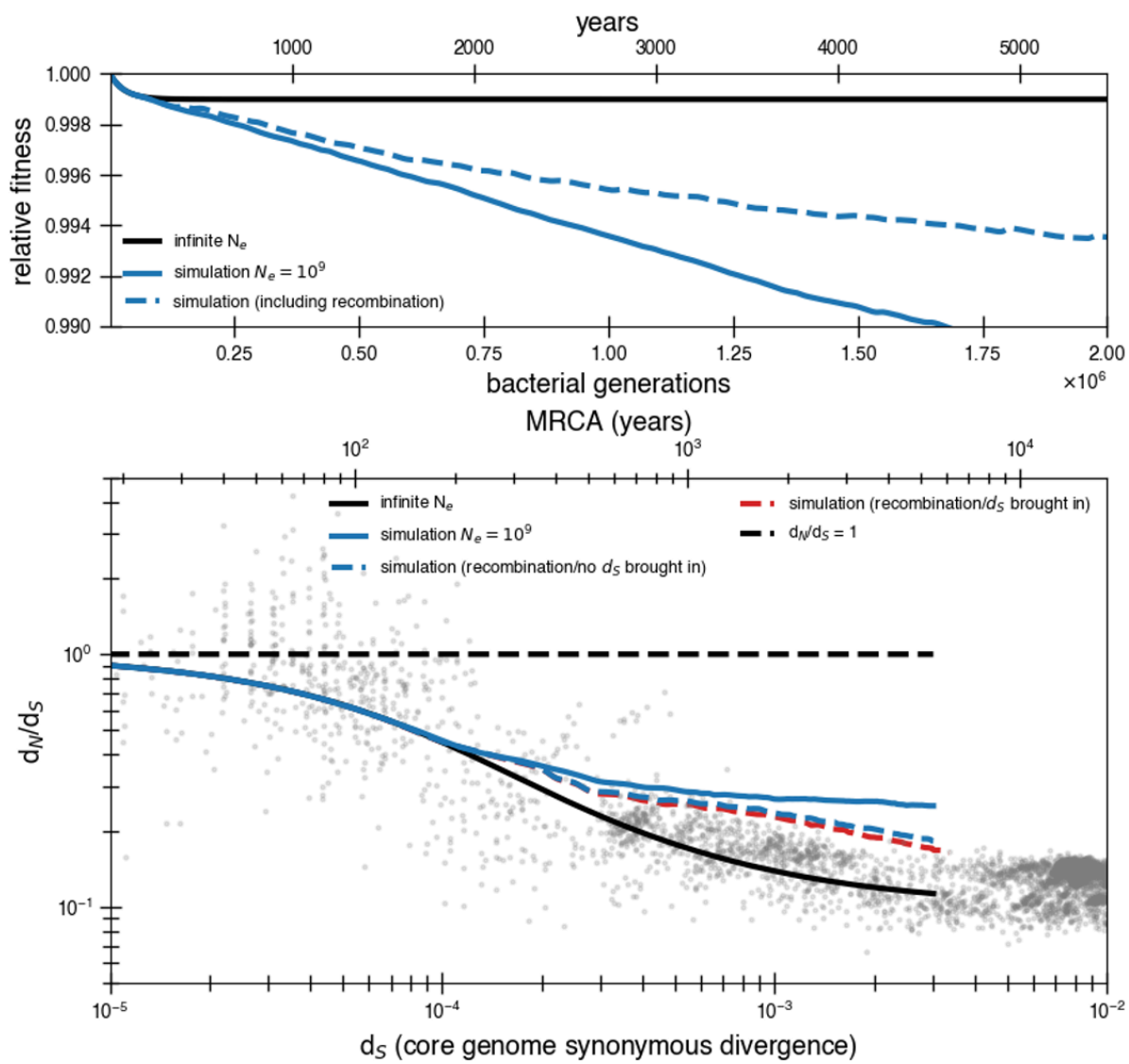

Figure S6: High rates of recombination are unlikely to rescue the purifying selection model. A purifying selection simulation with a population of 10^9 with and without recombination. To simulate the potential for recombination to lower mutational load, we assume 2.5×10^{-7} chance per codon per generation of return to the ancestral state (500 times the basal mutation rate, dotted blue line). All other assumptions are the same as the continuous selection simulations in Fig 2. While recombination does allow more fit genotypes to arise, their selective advantage is quite small and time to sweep is still slower than mutation accumulation. Recombination is more effective at purging deleterious alleles when many deleterious mutations are present, but this occurs at a longer timescale than the actual drop off of d_N/d_S values. We also include a variant where for every deleterious mutation reverted, a synonymous mutation is allowed to hitchhike with it to represent the possibility of recombined fragments coming from distant genomes. This would represent recombination bringing in fragments of 100 bp in length from a genome with d_S =0.01. This makes d_N/d_S drop slightly but not significantly.

1197

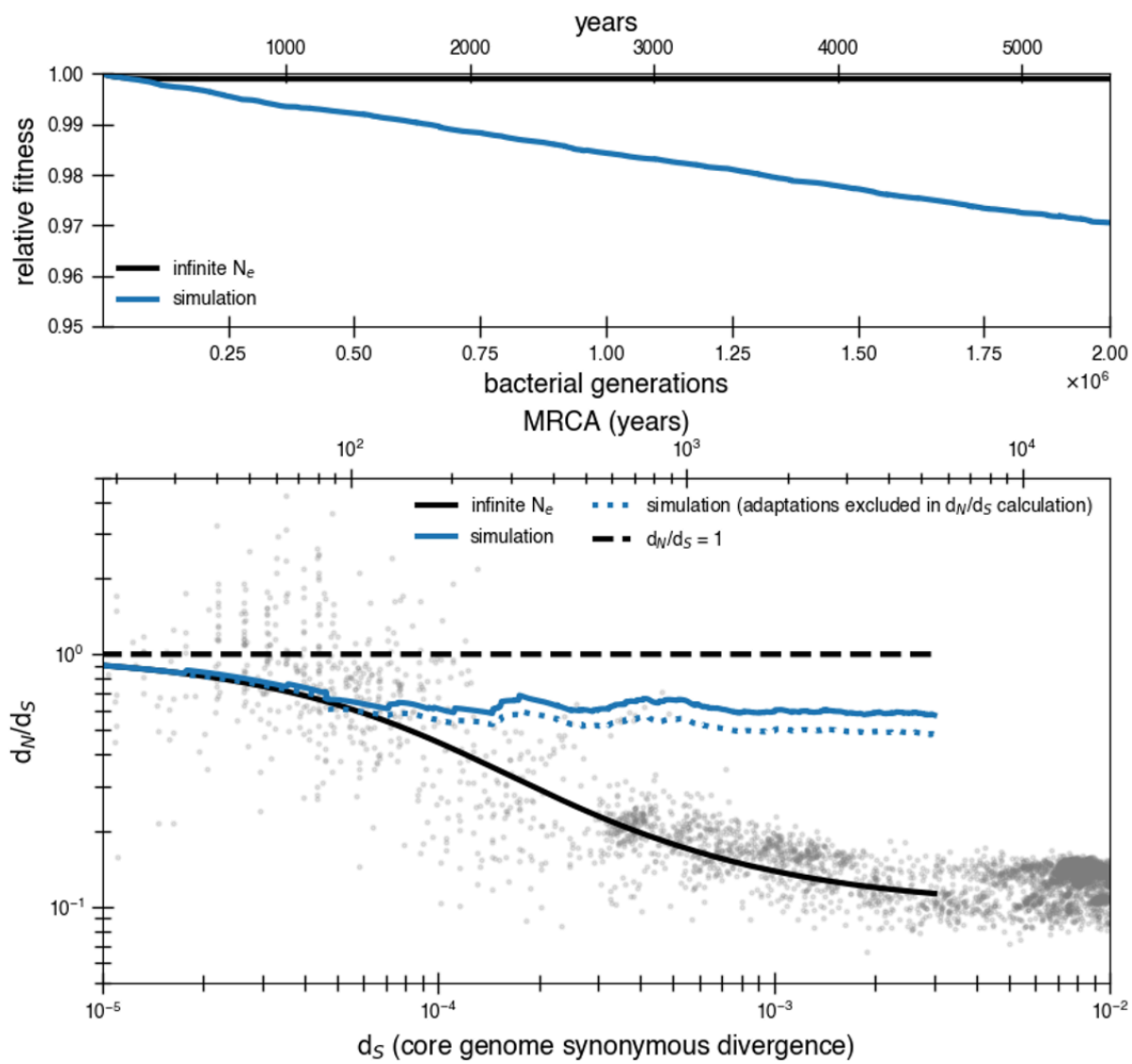

Figure S7: **Transmission bottlenecks and adaptation further complicate purifying selection.** Results of a simulation with purifying selection that take into account transmission bottlenecks and the possibility of adaptation. The simulation is meant to represent a potential transmission chain from gut to gut. This simulation is a modified version of the simulation used for the reversion model (see Methods). Only forward mutations are available when beneficial mutations arrive ($s_{ben} = 0.03$) and deleterious mutations arrive at a rate of 1.01 $\times 10^{-3}$ mutations per genome with a selective disadvantage of $s = 3.5 \times 10^{-5}$. The census size in an individual gut is 10^{10}. We choose very conservative values for adaptation rate, bottleneck size, and bottleneck frequency to show how even small levels of these dynamics strongly influence results. Transmission bottlenecks happen on average every 100,000 generations. The population is bottlenecked to 1,000 members upon transmission. Beneficial mutations are released on average every 8,400 generations. Multiple beneficial mutations can occur together (the number released at a time is a Poisson random variable of mean 1). This rate of beneficial mutation does not contribute much to d_N/d_S on its own as seen from the dotted line where adaptations are excluded in the d_N/d_S calculation. However, both of these scenarios drastically increase the rate of mutation accumulation and the

asymptotic d_N/d_S. The reversion model is able to prevent this from occurring with 10 times the amount of adaptation and transmission.

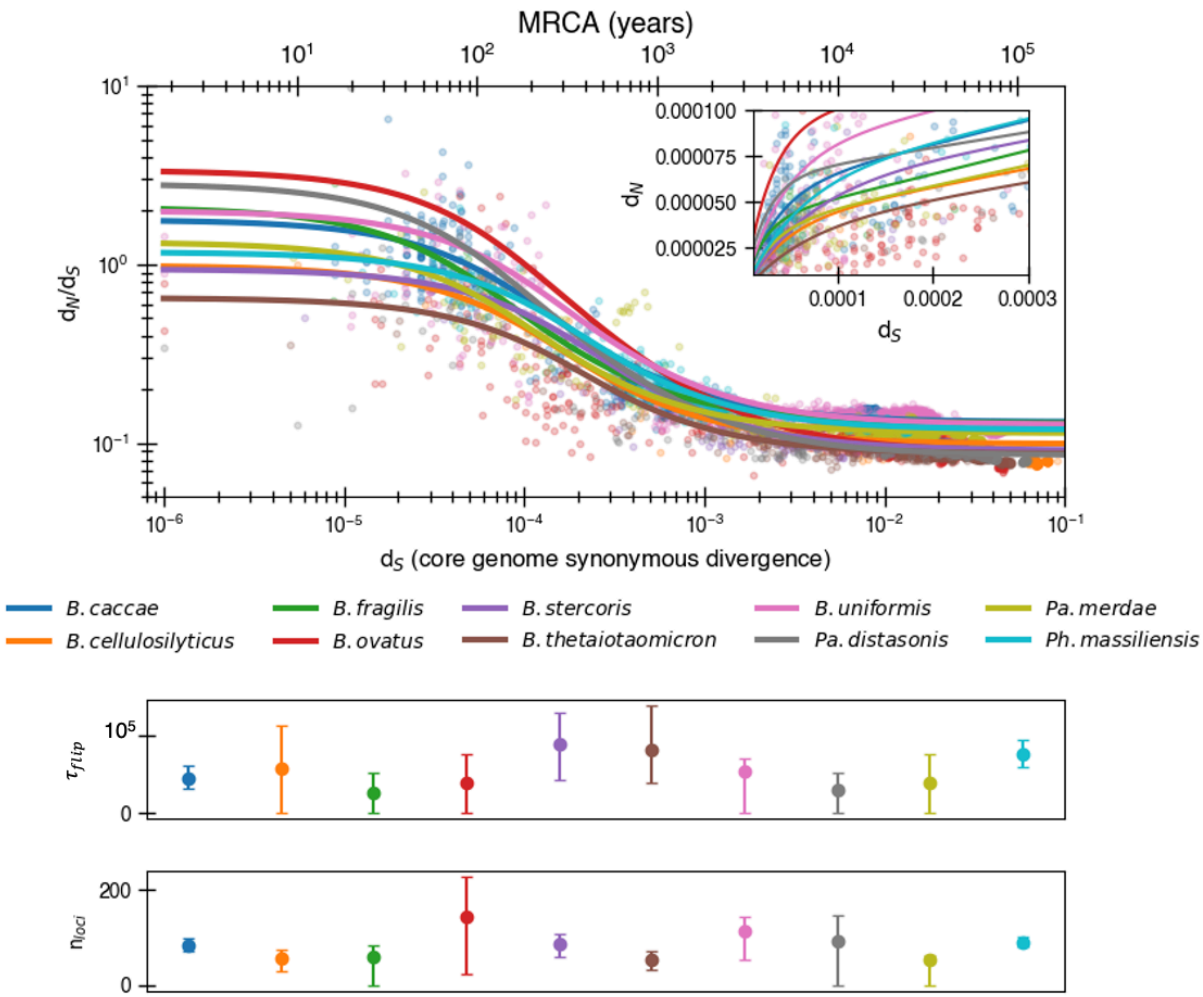

Figure S8: Potential for even more adaptation if fitting non logarithmic d_N/d_S. Results of fitting the reversion model (Equation 8) to minimize d_N/d_S rather than logarithmic d_N/d_S. This implies potential longer time to a switch a given selective pressure (median $\tau_{flip} = 53,340$) and an increased number of loci undergoing fluctuating selection (median $n_{loci} = 84$). The median R^2=0.72 (range: 0.11-0.88).

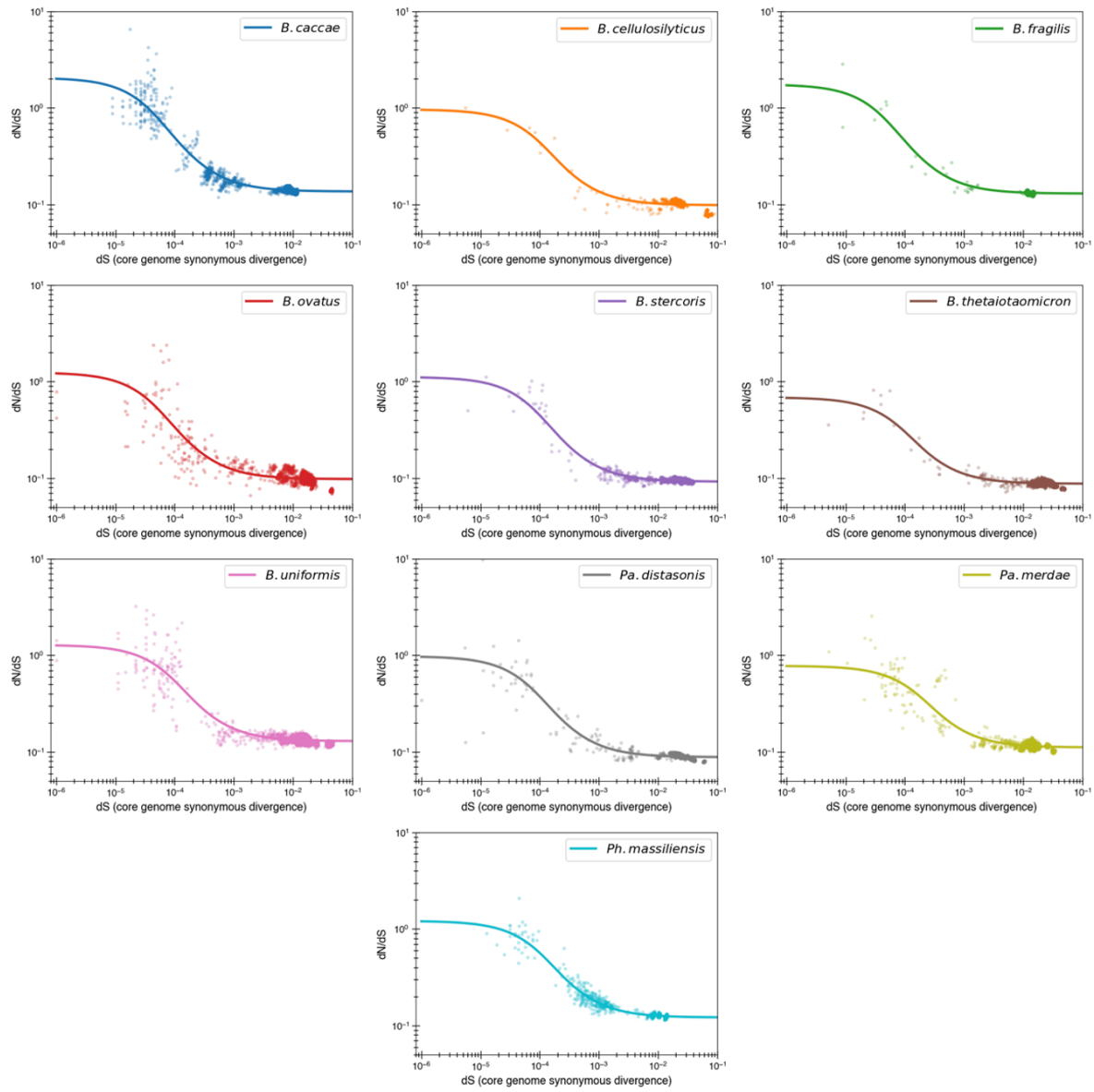

Figure S9: Reversion model fits by individual species. Content of Fig. 3b with each species now given its own panel. One species of note is *B. caccae* which appears to have initial d_N/d_S values above 1 which can now be fit with the reversion model (see Fig. S2 for comparison with purifying model).

1200

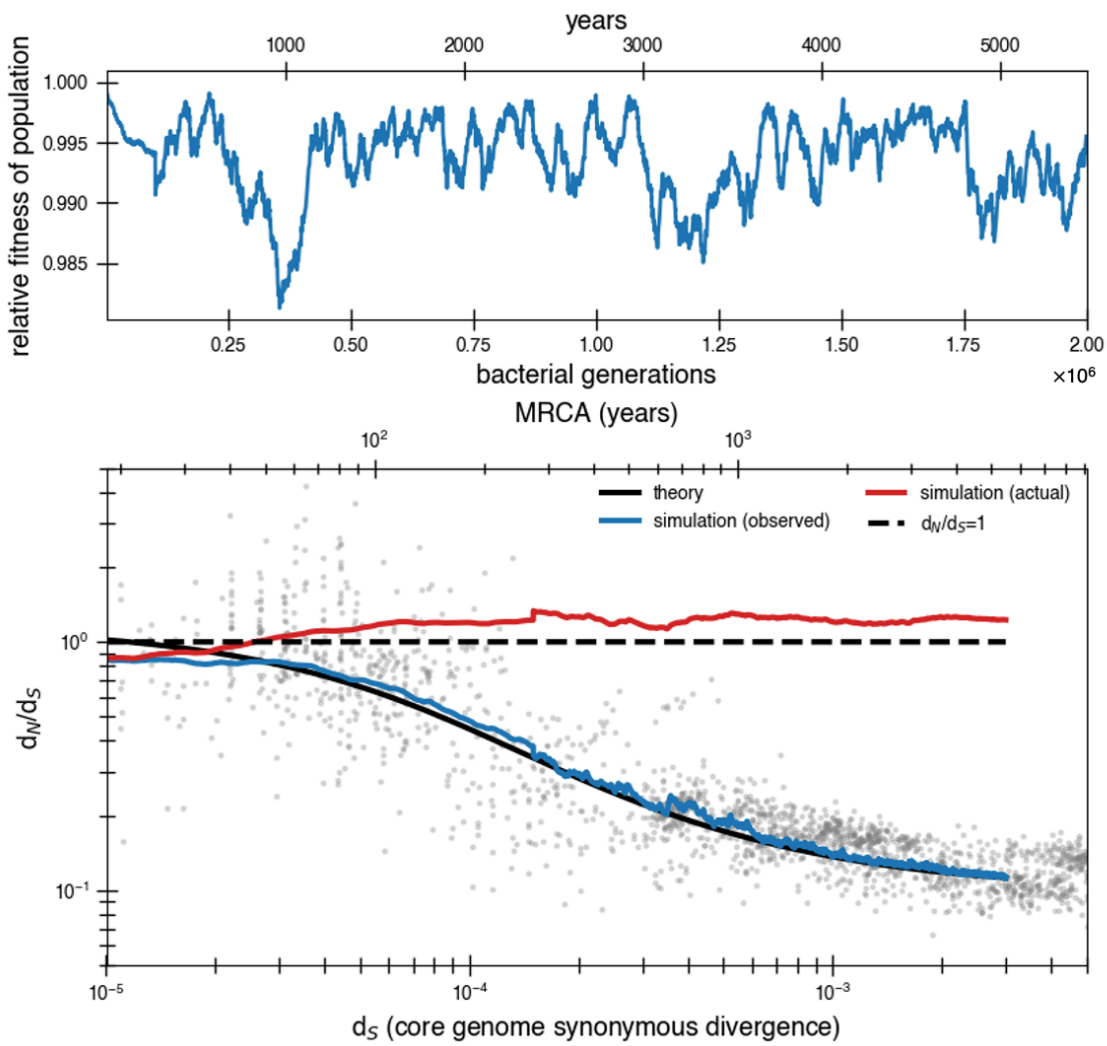

SI Figure 10: Effect of correlating mutations with bottleneck has little impact on the fit. Same parameters as simulation from Fig. 4a but rather than have new potential beneficial mutations occur independently of bottlenecks, they occur concurrently. In order to have an overall average of one beneficial mutation every 840 generations, an average of 11.9 mutations (Poisson with mean 11.9) occur every bottleneck, which occurs on average every 10,000 generations. The most noticeable difference is greater variability at low synonymous divergence values. The first 100,000 generations is the average of 50 simulations while subsequent parts of the curve consist of only 5 simulations to save on computing time (hence the slight spike).

1201

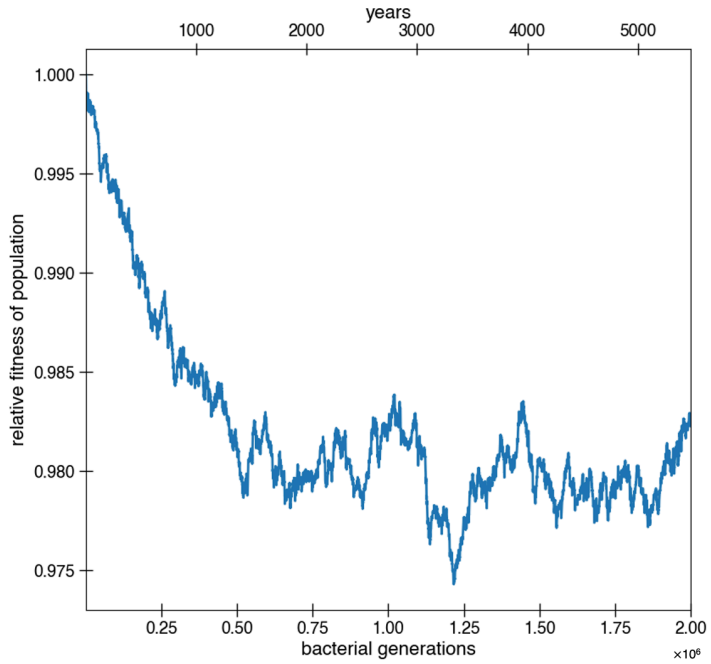

Figure S11: **Deleterious hitchhikers are reverted over time, preventing fitness decay.** Besides for reversions potentially occurring due to strong environmental pressures, reversions can also occur because of fixation of deleterious hitchhikers. These results are from the simulations of Fig 4a, where deleterious mutations occur at a rate of 1.01×10^{-3} per genome per generation and with a selective disadvantage of $s = 0.003$. Deleterious mutations are allowed to hitchhike, and reversions of these deleterious mutations are also permitted. Adaptive mutations and reversions are not counted in relative fitness. The curve is the average of 10 simulations.

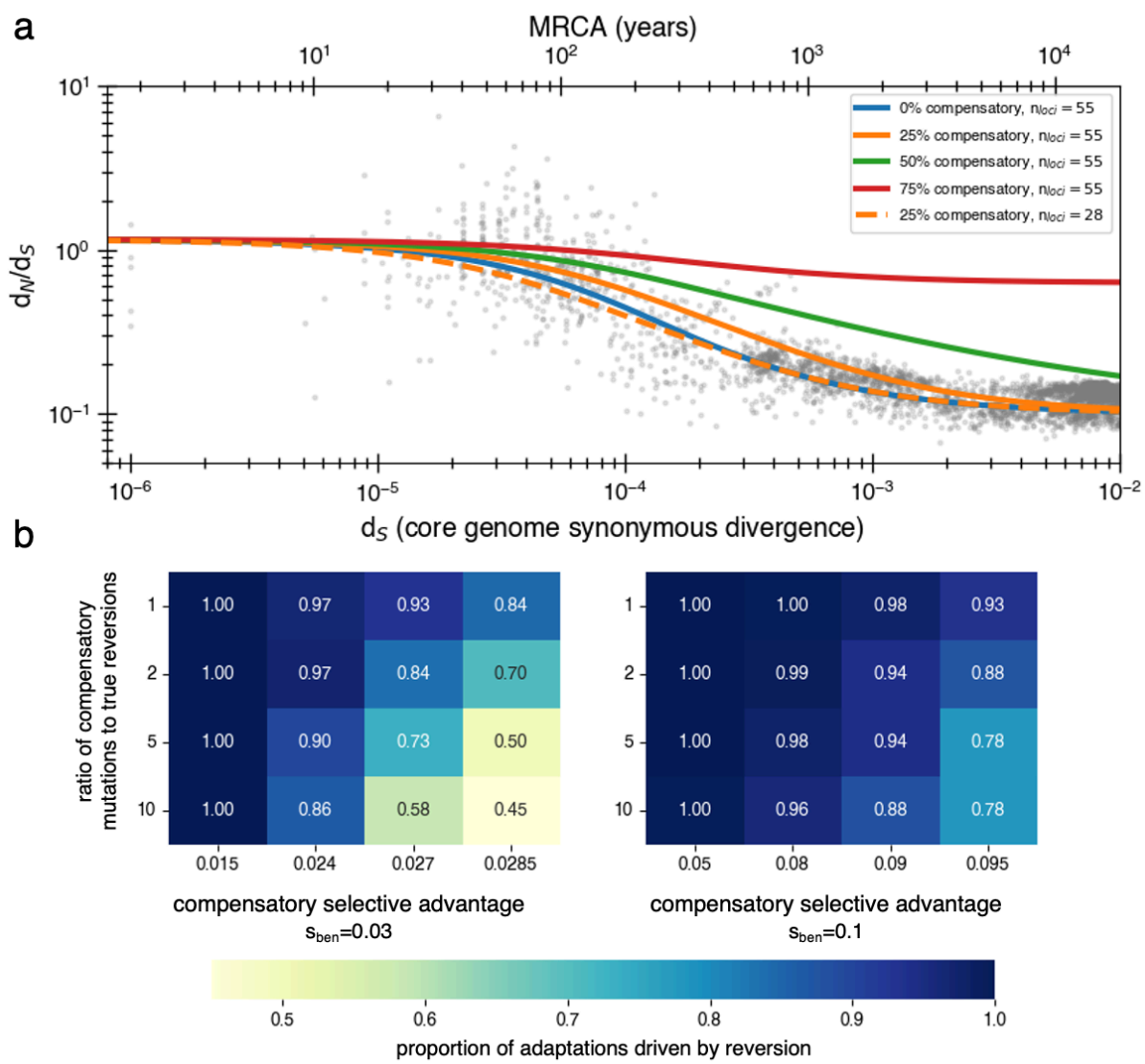

Figure S12: Inclusion of compensatory mutation in the reversion model shows that dN/dS still decays provided reversion occurs at reasonable rates. (**a**) Using a Markov chain (SI Text 3.2) we calculate the theoretical values of $\overline{N}_{transient}$, and thus d_N/d_S decay, under varying assumptions about the rate at which compensatory mutations win over true reversions. While compensatory mutations do slow the rate at which d_N/d_S decays (relative to no compensatory mutations), if reversions are more likely than compensatory mutations, a decay will be observed. Reducing the number of loci can correct for delayed decay from compensatory mutations. (**b**) The likelihood of true reversion vs. compensatory mutations (treated as mutually exclusive) under different parameter regimes as determined from simulations. Simulations are performed the same as those displayed in Fig 4 and described in the methods section for the reversion model (same population size, bottlenecks, loci, arisal of beneficial mutations, mutation rates), except now there is an additional compensatory category which can be used to satisfy an adaptation to a reverse pressure and has a separate rate and selective advantage. Results are obtained by comparing accumulated true reversions to compensatory mutations after 500,000 generations.